Signaling through cAMP-Epac1 induces metabolic reprogramming to protect podocytes in glomerulonephritis

Lilia Abbad, Maximin Détrait, Panagiotis Kavvadas, Dorian Bergonnier, Lisa Melis, Marion Laudette, Tiffany Migeon, Marie-Christine Verpont, Alexandre Lucas, Christos Chatziantoniou, et al.

▶ **To cite this version:**

Lilia Abbad, Maximin Détrait, Panagiotis Kavvadas, Dorian Bergonnier, Lisa Melis, et al.. Signaling through cAMP-Epac1 induces metabolic reprogramming to protect podocytes in glomerulonephritis. Kidney International, 2024, Online ahead of print. 10.1016/j.kint.2024.05.010 . hal-04610369

HAL Id: hal-04610369
https://edf.hal.science/hal-04610369v1

Submitted on 13 Jun 2024

HAL is a multi-disciplinary open access archive for the deposit and dissemination of scientific research documents, whether they are published or not. The documents may come from teaching and research institutions in France or abroad, or from public or private research centers.

L'archive ouverte pluridisciplinaire **HAL**, est destinée au dépôt et à la diffusion de documents scientifiques de niveau recherche, publiés ou non, émanant des établissements d'enseignement et de recherche français ou étrangers, des laboratoires publics ou privés.

Signaling through cAMP-Epac1 induces metabolic reprogramming to protect podocytes in glomerulonephritis

Lilia Abbad[1 *], Maximin Détrait[2 *], Panagiotis Kavvadas[1], Dorian Bergonnier[2], Lisa Melis[1], Marion Laudette[2], Tiffany Migeon[1], Marie-Christine Verpont[1], Alexandre Lucas[2], Christos Chatziantoniou[1 *], Frank Lezoualc'h[2 *]

[1]INSERM UMR S 1155, Common and Rare Kidney Diseases, Tenon Hospital, Faculty of Health, Sorbonne University, 75020 Paris, France.

[2]Institut des Maladies Métaboliques et Cardiovasculaires, INSERM, University Toulouse III-Paul Sabatier, UMR 1297-I2MC, 31432 Toulouse, France

LA and MD contributed equally to this article as first authors

CC and FL contributed equally to this article as last authors

Running headline: Epac1-induced glycolysis: a protective pathway for CKD

Abstract word count: 258

Text word count: 4063

Correspondence to:

Christos Chatziantoniou
Inserm UMR S 1155,
Tenon Hospital,4, rue de la Chine
75020 Paris, France
christos.chatziantoniou@sorbonne-universite.fr

or

Frank Lezoualc'h
Inserm UMR 1297, I2MC,
Univ de Toulouse III-Paul Sabatier
31432 Toulouse, France
Frank.Lezoualch@inserm.fr

Abstract

Unlike classical protein kinase A, with separate catalytic and regulatory subunits, EPACs are single chain multi-domain proteins containing both catalytic and regulatory elements. The importance of cAMP-Epac-signaling as an energy provider has emerged over the last years. However, little is known about Epac1 signaling in chronic kidney disease. Here, we examined the role of Epac1 during the progression of glomerulonephritis (GN). We first observed that total genetic deletion of Epac1 in mice accelerated the progression of nephrotoxic serum (NTS)-induced GN. Next, mice with podocyte-specific conditional deletion of Epac1 were generated and showed that NTS-induced GN was exacerbated in these mice. Gene expression analysis in glomeruli at the early and late phases of GN showed that deletion of Epac1 in podocytes was associated with major alterations in mitochondrial and metabolic processes and significant dysregulation of the glycolysis pathway. *In vitro*, Epac1 activation in a human podocyte cell line increased mitochondrial function to cope with the extra energy demand under conditions of stress. Furthermore, Epac1-induced glycolysis and lactate production improved podocyte viability. To verify the *in vivo* therapeutic potential of Epac1 activation, the Epac1 selective cAMP mimetic 8-pCPT was administered in wild type mice after induction of GN. 8-pCPT alleviated the progression of GN by improving kidney function with decreased structural injury with decreased crescent formation and kidney inflammation. Importantly, 8-pCPT had no beneficial effect in mice with Epac1 deletion in podocytes. Thus, our data suggest that Epac1 activation is an essential protective mechanism in GN by reprogramming podocyte metabolism. Hence, targeting Epac1 activation could represent a potential therapeutic approach.

Keywords

Chronic kidney disease, Cyclic AMP signaling, Warburg effect, Glycolysis, Mitochondria function, Therapeutic approach.

Translational statement

Novel therapeutic strategies are urgently needed for chronic kidney diseases, especially for glomerular diseases. As activation of cAMP signaling is protective in several diseases, we investigated the role of the cAMP effector Epac1 in experimental glomerulonephritis. We found that Epac1 induces a reprogramming of podocyte metabolism towards glycolysis and lactate production as a protective mechanism against glomerular insult. Furthermore, we found that administration of an Epac1 agonist attenuates the progression of experimental glomerulonephritis, providing a first preclinical indication of a new therapeutic strategy based on pharmacological activation of Epac1 signaling.

Introduction

An estimated 700 million to one billion of people worldwide suffer from Chronic Kidney Disease (CKD), a major burden for public health, with glomerulonephritis (GN) being one of the most severe forms[1,2]. Many aspects of the complex mechanisms orchestrating the development of CKD have been identified and patient care has remarkably improved. Despite this progress, most forms of GN are progressive disorders, without timely therapeutic intervention, and constitute 25%-30% of all end-stage renal disease eventually leading to morbidity[3,4]. Therefore, identifying novel specific therapeutic targets against the progression of GN and of renal disease in general is one of the major challenges of public health today.

Cyclic AMP (cAMP) is a universal and versatile second messenger, and its production is initiated upon activation of membrane-bound and/or soluble adenylyl cyclases which generate intracellular level of cAMP[5]. Dysregulation of cAMP signaling is associated with numerous disorders including the renal and cardiovascular systems[6,7]. Besides the classical protein kinase A (PKA) signaling route, exchange proteins directly activated by cAMP (Epac1 and Epac2) mediate the biological action of cAMP, acting as guanine exchange factors for the small G-proteins Rap1 and Rap2, and function in a PKA-independent manner[8–10]. Recent evidence indicates increased Epac1 expression and signaling during the development of various pathologies including heart failure and cancer[11,12].

While Epac1 is expressed in the kidney[8], its role in renal physiology and pathophysiology has been delineated to a limited extent and to date most studies have been performed in *ex vivo* or *in vitro* settings using the synthetic Epac1 preferential agonist 8-pCPT[12]. Epac1 has been implicated in the regulation of the Na^+/H^+ exchanger 3 activity in proximal tubules, and the Na^+ channel activity and urea transport in inner medullary collecting duct[13–16]. In addition, Epac1 activation with 8-pCPT protected the epithelial barrier function against hypoxia *in vitro*[17,18]. Consistently, activation of Epac-Rap signaling reduced

ROS production and cell death in a mouse model of ischemia-reperfusion injury[18]. In the present study, we assessed the role of Epac1 in an experimental model of GN, using a combination of genetic and pharmacological approaches. In addition, glomerular transcriptomics (RNA sequencing) and podocyte metabolism (Seahorse) analysis led us to determine that Epac1 signaling induces a Warburg-like metabolic reprogramming in podocytes as a protective mechanism against glomerular injury.

Materials and Methods

Animal experiments

All mice were handled in strict accordance with good animal practice as defined by the relevant national animal welfare bodies of France, and all animal work was approved by the appropriate committee of the Inserm and Sorbonne University. Animals were housed at constant temperature with access to water and food ad libitum. For all experiments, passive GN was induced in 3-month-old female mice, by 2 consecutive days' intravenous injections of decomplemented nephrotoxic serum (NTS), prepared as previously described[19,20]. Control mice were injected with PBS. Epac1-deficient mice (Epac1$^{-/-}$) have been generated in our laboratory as previously described[21]. NTS was administered in Epac1$^{-/-}$, conditional knockdown mice with Epac1 deletion specifically in podocytes (*NPHS2Cre*: Epac1$^{fl/fl}$) and their littermate controls. The Epac1 agonist 8-pCPT was administered in wild-type or *NPHS2Cre*: Epac1$^{fl/fl}$ mice treated with NTS. In the results, figures and legends sections, the littermates control mice for Epac1$^{-/-}$ were annotated as wild-type (WT) and for *NPHS2Cre*: Epac1$^{fl/fl}$ as control (Ctr). More details are provided in the Supplementary Methods.

Glomeruli Isolation and RNA extraction for RNA sequencing

Glomeruli were isolated from conditional (*NPHS2-Cre*: Epac1$^{fl/fl)}$ and control littermate mice injected with PBS or NTS at two time points: in the early phase (day 4) or later phase (day 11) of disease. Glomeruli were isolated from 10 µM cryosections by laser microdissection (Arcturus XT, Exilon), collected on Cupules (Excilone) and RNA was isolated. Details for RNA sequencing and bioinformatics analysis are given in the Supplementary Methods.

Measurements of oxygen consumption and extracellular acidification rate

An Agilent Seahorse XF Pro Analyzers was used to measure the rate change of dissolved O_2 and pH in medium immediately surrounding adherent cells cultured in a Seahorse XFe96 Analyzer 96-well plate (Seahorse Agilent). Detailed description is given in the Supplementary Methods.

Podocyte cell culture, cell viability test and Scratch assay are described in Supplementary methods

Statistical analysis

Values are expressed as mean ± SEM. Difference among groups was determined by One-way or Two-way ANOVA followed by Tukey multiple comparisons test or Kruskal-Wallis test followed by Dunn's multiple comparisons test, if normality was not respected, using GraphPad Prism version 9.5.0 (GraphPad Software). Data were considered statistically significant when p-value < 0.05.

Results

Epac1 deficiency is associated with accelerated decline in renal function in NTS-induced GN

Epac1 is expressed in kidneys and particularly glomeruli of wild type (WT) animals under normal conditions, whereas it is absent in mice lacking Epac1 expression ($Epac1^{-/-}$) (Figures 1a, b). To determine whether Epac1 has a functional role in CKD development, GN was induced in mice $Epac1^{-/-}$ using their WT littermates as controls (Figure 1c). This experimental model of acute GN produces a severe nephropathy in mice, independently of the genetic background, leading to end-stage-renal-disease after 15-20 days[22]. $Epac1^{-/-}$ mice do not show alterations of renal function and structure in basal conditions (Figure 1). In addition, equivalent amounts of goat IgG and mouse IgG deposits were found in glomeruli from WT and $Epac1^{-/-}$ mice after NTS injections (Supp Figure S1). As expected, NTS administration progressively impaired renal function in WT mice as evidenced by the increased proteinuria and blood urea (Figures 1d, e). $Epac1^{-/-}$ mice showed an accelerated decline of renal function compared with NTS-treated WT animals (Figures 1d, e) suggesting that Epac1 deficiency potentiates the deterioration of renal structure and function in GN.

Deletion of Epac1 is associated to exacerbated renal fibrosis, inflammation and damage in GN

As expected, markers of fibrosis such as collagen I or α-SMA and of renal damage such as kidney injury molecule-1 (KIM-1) or neutrophil gelatinase–associated lipocalin (NGAL, were highly increased following NTS in WT mice (Figures 1f, 2). This increase was amplified in NTS-treated $Epac1^{-/-}$ mice (Figures 1f, 2). In addition, this group of mice showed increased glomerular crescent formation and tubular damage compared with the WT+NTS group (Figure 3, left panels). F4/80 immunostaining indicated an aggravated macrophage infiltration

in the renal cortex of Epac1$^{-/-}$+NTS (Figure 3, middle). The monocyte chemoattractant (MCP-1) and the vascular cell molecule adhesion 1 (VCAM-1), both crucial for monocyte/macrophages adhesion, migration and infiltration, were further increased in kidneys of Epac1$^{-/-}$+NTS mice (Figure 1f). Podocyte injury was confirmed by the down-regulated expression of the podocyte-specific marker William's Tumor-1 (WT-1) (Figure 3, right panels). These data show that deletion of Epac1 expression markedly potentiated glomerular injury and renal inflammation in GN.

Podocyte-specific knock-down of Epac1 expression accelerates the development of NTS-induced GN

Subsequently, we confirmed that Epac1 is expressed in podocytes of WT mice by co-localizing Epac1 with nestin, a marker of podocytes (Figure 4a, upper panels). This observation together with the exacerbated proteinuria reported in Epac1$^{-/-}$ mice (Figure 1), led us to investigate the effect of the specific inactivation of Epac1 in podocytes during GN (Figure 4b). To this end, we generated a mouse strain with conditional Epac1 deletion in podocytes (*Nphs2Cre*-Epac1$^{fl/fl}$, see Methods). Immunofluorescence confirmed almost complete deletion of Epac1 expression in podocytes of *Nphs2Cre*-Epac1$^{fl/fl}$ mice (Figure 4a, lower and right panels, Supp Figure S2). Parameters of renal function such as proteinuria, blood urea, plasma creatinine (Figures 4c-e), markers of fibrosis and renal damage (Figure 5), histology and podocyte morphology (Figure 6, upper panels) were normal in these mice under basal conditions. However, following NTS administration, the decline of renal function was exacerbated in *Nphs2Cre*-Epac1$^{fl/fl}$ mice (Figures 4c-e), and gene or protein expression markers of fibrosis (collagen I), renal damage (KIM-1, NGAL) and inflammation (MCP-1, VCAM-1) were significantly augmented compared with Ctr+NTS mice (Figure 5). In line with these data, histological analysis showed a further increase of crescent formation and

macrophage infiltration in *Nphs2Cre*-Epac1$^{fl/fl}$ mice (Figure 6, left and middle panels). The severe glomerular injury was also accompanied by major alterations in podocyte structure. Electronic microscopy showed important thickening of glomerular basement, vacuolization, and foot process effacement in glomeruli from NTS-treated *Nphs2Cre*-Epac1$^{fl/fl}$ mice (Figure 6, right lower panel). Podocyte disorganization was also shown by the absence of slit diaphragm in most cases. Ctr mice treated with NTS displayed alterations in podocyte structure, but to a lesser degree (Figure 6, right). Thus, Epac1 deficiency in podocytes does not cause an abnormal renal phenotype under control conditions, but aggravates the progression of GN.

Transcriptomic signature underlying NTS-induced GN

To determine the pathways responsible for the kidney susceptibility to GN, RNA sequencing (RNAseq) was performed on mRNAs extracted from glomeruli of Ctr or *Nphs2Cre*-Epac1$^{fl/fl}$ mice treated or not (PBS) with NTS (Figure 7a). As this is bulk RNA analysis, the transcriptional changes correspond to the whole glomerulus and cannot be localised to podocytes. Two different time-points of glomerular microdissection were chosen: at 4 or 11 days after NTS corresponding to the early or established phase of GN, respectively. Firstly, we analyzed the transcriptomic signature of the GN model. Comparison analysis of NTS Ctr versus PBS Ctr mice identified 269 and 427 differentially expressed genes (FDR < 0.05) at day 4 and day 11, respectively (Supp Figures S3a-d). Pathway enrichment analysis using Gene Ontology database showed that NTS-induced GN dysregulated biological process terms related to immune system and metabolism at day 4 (Supp Figure S4a) and to developmental process, cell cycle and cell division at day 11 (Supp Figure S4b). Consistent with the involvement of cAMP-Epac1 axis in GN development, G protein-coupled and adenylate cyclase-activating G protein-coupled receptor pathway terms were dysregulated from the

early stage of the disease (Supp Figures S4). Concerning cellular compartment, at day 4, the analysis revealed dysregulated terms associated to extracellular matrix, cytoskeleton and membrane protein complex. These terms were even more dysregulated at the late phase of the disease (Supp Figure S5).

This transcriptomic signature, showing major alterations in genes involved in immune system, extracellular matrix and cytoskeleton, is consistent with the phenotypic analysis of the NTS-induced GN and validates our model and analysis. In addition, these data revealed that major metabolic changes occur in the glomeruli at the onset of GN.

Deletion of Epac1 in podocytes induces further alterations in mitochondria and metabolic processes at the onset of GN

Comparison of RNAseq data from Ctr NTS and *Nphs2Cre*-Epac1$^{fl/fl}$ NTS mice provided clues to determine the impact of podocyte Epac1 deletion on genes and pathways regulating GN progression. Comparison of Ctr and *Nphs2Cre*-Epac1$^{fl/fl}$ mice identified 121 and 134 differentially (FDR < 0.05) expressed genes at day 4 and 11 after NTS, respectively (Supp Figure S6).

The absence of Epac1 worsened the dysregulation of metabolic process terms in the early stage of GN (Figure 7b). Among these metabolic processes, glycolysis and fatty acid metabolism related genes were downregulated in *Nphs2Cre*-Epac1$^{fl/fl}$ +NTS mice (Figure 8a, Supp Figure S7). In addition, Epac1 deletion was associated with mitochondria and membrane protein complex modifications (Supp Figure S8a) suggesting that these metabolic alterations contribute to aggravate the pathological phenotype of GN.

Metabolic and mitochondrial terms became less prevalent in the *Nphs2Cre*-Epac1$^{fl/fl}$ mice at day 11 (Figure 7c): the above-mentioned alterations in glycolysis and fatty acid metabolism pathways were similar in the two groups, whereas only the mitochondrial oxidative

phosphorylation pathway was further downregulated (Figure 8b). Consistent with the molecular and histological analysis of *Nphs2Cre*-Epac1$^{fl/fl}$ mice (Figures 4-6), apoptotic, immune system, cytoskeleton, extracellular region, membrane protein complex and protein-containing complexes (such as collagen) were modified at day 11 (Figure 7c; Supp Figure S8b).

Thus, the RNAseq analysis showed that the absence of Epac1 in podocytes is accompanied by major alterations of gene patterns involved in glycolysis and mitochondrial function at the onset of GN. These alterations could contribute to exacerbate glomerular injury and aggravate the progression of GN.

Epac1 activation improves mitochondrial function of podocytes

Since oxidative stress is an important trigger of NTS-induced renal injury[23,24], the role of Epac1 in hydrogen peroxide (H_2O_2)-mediated podocyte injury was evaluated using the human Ab8/13 podocyte cell line. As expected H_2O_2, decreased cell viability and motility, whereas the Epac1 specific agonist 8-CPT-AM prevented the H_2O_2-induced cell injury (Figures 9a-c).

Because mitochondrial respiration and metabolism are essential for podocyte bioenergetics[25] and since the RNAseq analysis indicated that Epac1 is involved to oxidative phosphorylation and mitochondrial ATP synthesis coupled proton transport (Figures 7, 8), next we investigated the role of Epac1 in podocyte respiration.

Using Seahorse analyzer, cellular oxygen consumption rate (OCR), an index of mitochondrial respiration, was measured in cells treated or not with H_2O_2 and/or 8-CPT-AM (Figure 9d). Epac1 activation exacerbated the decrease of cellular respiration and mitochondrial ATP production induced by H_2O_2 (Figures 9e, f). This was not due to an effect of H_2O_2 or 8-CPT-AM on the number of mitochondria, but rather on mitochondrial function (Supp Figure S9a). Indeed, the decline in basal respiration and ATP production (Figures 9e, f) was correlated

with a change in the spare respiratory capacity (SRC, also named mitochondrial reserve capacity). SRC represents the percentage between maximal OCR and basal OCR, reflects the capability of the cells to respond to changes in energetic demand, and thus characterizes the mitochondrial capacity to meet extra energy requirements in response to a given cellular stress[26]. 8-CPT-AM alone or in combination with H_2O_2, largely increased SRC compared with the control DMSO or H_2O_2 (Figure 9g). Consistent with this finding, the decrease of proton leak reflecting mitochondrial efficacy and integrity was further reduced by 8-CPT-AM in the presence of H_2O_2 (Figure 9h). Altogether these data suggest that Epac1 activation enhances mitochondrial reserve and efficacy thereby helping podocytes to cope with higher energy demand in response to stress.

Epac1 promotes glycolysis to protect podocytes from oxidative stress

Podocytes with Epac1 deletion displayed decreased glycolysis-associated genes at the onset of GN (Figure 8a). Since glycolysis is known to compensate impaired mitochondrial function in podocytes[25], the role of Epac1 on glycolytic pathway was subsequently investigated. Podocytes treated with either 8-CPT-AM alone or in combination with H_2O_2 displayed increased glycolysis as assessed by measuring extracellular acidification rate (ECAR) with Seahorse analyzer (Figures 10a, b).

The end-product of glycolysis is pyruvate, which can be either oxidized in the mitochondria or fermented to lactate. To further characterize the impact of pyruvate metabolism in podocytes, the contribution of glucose oxidation (glucose dependency) to mitochondrial respiration was measured using UK-5099, a mitochondrial pyruvate carrier inhibitor. Glucose oxidation mainly contributes to mitochondrial respiration in basal conditions (Figure 10c). Although H_2O_2 treatment did not influence glucose dependency, the addition of 8-CPT-AM decreased mitochondrial glucose oxidation (Figure 10c). In return, 8-CPT-AM shifted to fatty

acid oxidation (Supp Figure S9b). This consolidates the observation that Epac1 deletion dysregulated fatty acid related genes at the onset of GN (Supp Figure S7). The increase in lactate concentration induced by 8-CPT-AM (Figure 10d), shows that the pyruvate that was not oxidized by mitochondria, was fermented to lactate.

It appears thus, that Epac1 activation protects podocytes from H_2O_2-mediated oxidative stress through an increase in glycolysis and lactate production. In favor of this hypothesis, 2DG, an inhibitor of glycolysis, abolished the beneficial effect of 8-CPT-AM on cell viability and migration of H_2O_2-treated podocytes (Figures 10e, f).

These data show that Epac1 activation reprograms podocyte metabolism and induces glycolysis with a shift of pyruvate utilization from the mitochondria towards lactate fermentation, and by doing so it protects podocytes from cell stress (Figure 10g).

Therapy relevance: Pharmacological activation of Epac1 slows the progression of GN

Next, we determined whether Epac1 activation *in vivo* after the onset of the disease, could have beneficial effects on renal function. To this end, on day 3 of the protocol (Figure 11a), WT mice were treated with 8-pCPT or vehicle until the end of experiments (day 15). As shown in Figures 11b and c, 8-pCPTadministration mitigated proteinuria and the increase of plasma creatinine. This functional improvement was associated with a decreased formation of crescents and a better preservation of renal structure (Figure 11d, left panels). Macrophage infiltration was reduced in the renal cortex of 8-pCPT-treated mice and WT1 expression was preserved (Figures 11d, middle and right panels), further demonstrating the protective effect of Epac1 activation against NTS-induced GN.

The beneficial effect of pharmacological activation of Epac1 depends on podocytes

Finally, to determine whether the protective effect of 8-pCPT depends on the activation of Epac1 in podocytes, on day 3 of the protocol, Nphs2Cre-Epac1fl/fl mice or their Ctr were treated with 8-pCPT or a vehicle until the end of the experiments (day 15, Figure 12a). Analysis of renal function and structural parameters showed a similar profile of GN progression in both groups (Figures 12b-e). It therefore appears that treatment with 8-pCPT is not effective in the absence of Epac1 in the podocytes.

Discussion

The major novel finding of the present study is the identification of the cAMP-Epac1 signaling as a novel renoprotective pathway in experimental acute GN. Specifically, we found that the total genetic deletion of Epac1 expression potentiated renal inflammation and interstitial fibrosis, and accelerated the decline of renal function in NTS-induced GN, rendering thus mice more susceptible to progress towards end-stage-renal-disease. In addition, podocyte-specific deletion of Epac1 expression exacerbated the progression of GN to a similar degree as with the total deletion, thereby revealing a crucial role for Epac1 in podocyte damage. Mechanistically, the absence of Epac1 was associated with major dysregulation in pathways related to cell energy metabolism. Conversely, its activation preserved mitochondria, redirected metabolism towards glycolysis and protected podocytes from stress-induced damage. Administration of 8-pCPT, a specific Epac1 agonist, during early GN improved renal function and protected kidneys of WT mice against fibrosis, inflammation and structural damage. In contrast, 8-pCPT had no beneficial effect in mice lacking Epac1 expression in podocytes. Previous studies have shown that drugs increasing cAMP levels prevented inflammation and improved renal function and histology in lupus nephritis[27], but to the best of our knowledge, this is the first study investigating the effect of Epac1 signaling in experimental acute GN.

The observation that 8-pCPT had no beneficial effect in mice with Epac1 deletion in podocytes suggest an important role of local Epac1 activation. In the NTS model, renal damage is initiated in podocytes but progresses and affects all renal cell types and compartments. Damaged podocytes secrete stress signals such as chemo- and cytokines that activate cellular stress pathways inducing pathological phenotypic adaptations of neighbouring cells. Our hypothesis is that Epac1 activation in podocytes is an essential early event to maintain cell survival and attenuate disease progression. When this protective

mechanism is lacking, the pathology progresses more rapidly, affecting all parameters of renal function and structure. Mechanisms like this show the importance of improving cell-targeted therapy techniques and precision medicine approaches in kidney diseases.

The protection induced by the Epac1 agonist is consistent with previous studies showing a beneficial effect of Epac1 agonists in models of acute renal injury such as unilateral ureteral obstruction and ischemia/reperfusion injury[18,28]. In these studies, Epac1 agonists decreased reactive oxygen species (ROS) production and fibrosis in tubular epithelial cells. On the contrary, another study reported a protective effect of Epac1 inhibition in myocardial I/R damage in mice[29]. This differential effect suggests that the cAMP-Epac1 signaling is probably compartmentalized and could mediate distinct and even opposite cellular responses in a spatial-temporally regulated fashion[30]. Tissue-specific mechanisms of I/R can also explain this difference. Whatever the case, in our experiments systemic administration of 8-pCPT was protective and not accompanied by adverse effects.

Consistent with a role of Epac1 signaling in mitochondria[29,31], RNAseq analysis strongly suggested that the absence of Epac1 expression in podocytes dysregulated genes related to mitochondrial function at the onset of GN (Figures 7, 8). The mitochondrial capacity to rapidly produce extra energy, known as spare respiratory capacity (SRC), is not required in basal conditions. However, it is an important response mechanism in stress conditions, and maintaining high levels of SRC is correlated with cell resistance and survival[24]. Inversely, decrease in SRC levels indicates the inability of mitochondria to cope with extra energy demands and is associated to cell death[24]. Agents that preserve cells against loss in mitochondria SRC are considered to have a therapeutic potential[24,32]. Therefore, we tested whether selective activation of Epac1 protects podocytes from injury by improving mitochondrial function and increasing metabolic flexibility. Indeed, cell metabolism (Seahorse) and cell survival analysis revealed that Epac1 activation triggered mitochondrial

SRC in response to stress in human podocytes, promoting their survival. Despite this ability to induce extra mitochondrial energy, the fact that activation of Epac1 reduced oxidative phosphorylation and the resulting ATP production in podocytes (Figure 9e, f) implies metabolism reprogramming towards an alternative pathway, such as glycolysis.

Glycolysis and mitochondrial oxidative phosphorylation are the two main sources for ATP energy generation, glycolysis being approximately 100 times faster. To cope with energy demands, cells often switch between these pathways[33,34]. Here we report a new important finding, the Epac1-induced glycolysis in diseased glomeruli. Our RNAseq data show that deletion of Epac1 in podocytes resulted in dysregulation of genes linked to the glycolysis pathway at an early stage of GN, leading to exacerbation of the disease. In contrast, Epac1 activation increased glycolysis which promoted podocyte survival and improved renal function.

Glycolysis is known to be crucial for maintaining effective energy supply in podocyte foot processes[28]. Indeed, mitochondria have been described as being closer to the nucleus providing ATP in the cytosol, whereas ATP supply in lamellipodia is predominately provided by glycolysis to maintain podocyte structure and function[35,36]. Supporting this notion, inhibition of glycolysis through specific deletion of pyruvate kinase muscle 2 in podocytes aggravated glomerular injury in a model of nephrotic syndrome[37]. Conversely, overexpression of this enzyme in podocytes protected against albuminuria, mesangial expansion and podocyte foot process damage in a streptozotocin-induced model of diabetic nephropathy[38]. In addition, activation of another glycolytic enzyme, the phosphofructokinase PFKP, ameliorated foot process fusion in diabetic kidney disease[39]. These observations are consistent with our hypothesis that, to protect podocytes from stress conditions, Epac1 induces a metabolic reprogramming with glycolysis as the predominant metabolic pathway.

The Epac1-induced glycolysis and mitochondrial reserve were not associated to a higher rate of glucose oxidation, because mitochondrial ATP production and glucose dependency decreased (Figure 9f, 10c). In addition, fatty acid oxidation which is another source of energy production via the β-oxidation spiral, was largely increased upon Epac1 activation (Supp Figure S9b). These results agree with the notion that podocytes primarily utilize fatty acid oxidation as a protection mechanism from toxicity induced-lipid accumulation[40], whereas glucose oxidation impairs cell survival[41]. Moreover, we found that the Epac1-induced increased glycolysis combined with decreased glucose oxidation resulted in an augmentation of extracellular levels of lactate (Figure 10d). Instead of entering mitochondria, pyruvate derived from glycolysis is converted by the cytosolic enzyme lactate dehydrogenase to lactate[42]. The latter is crucial for energy generation[43], and represents a critical source of energy for podocytes in order to maintain the glomerular filtration barrier[43]. The steps of conversion of lactate to ATP production are simpler and faster than those involved in glucose oxidation[44]. Although for several years lactate production was considered as a waste end product of ischemic tissues, recent evidence promotes the notion of an alternative way of energy supplier to preserve tissue and cell homeostasis[45].

Our findings regarding the metabolic response of podocytes to GN induction resembles to the Warburg effect[46], characterized by a switch from oxidative phosphorylation to a rapid aerobic glycolysis associated with an increased production of lactate. Although this phenomenon is a major mechanism in cancer cells and tumor progression, emerging data indicate the presence of a Warburg-like effect in other tissues during pathophysiological conditions as well[47,48]. Normal rats subjected to high salt intake switched from the tricarboxylic acid cycle (TCA cycle) to glycolysis even though oxygen consumption augmented[49]. Increased glycolysis was evident by the upregulation of key glycolytic enzymes and release of pyruvate and lactate from the kidney in the renal venous blood. This Warburg-

like effect is proposed as a defense mechanism to cope with the needed increase in cellular energy and to protect the kidney from oxidative stress and injury[49].

In conclusion, our study demonstrates that Epac1 induces a metabolic reprogramming as a protective mechanism against rapidly progressing GN. Activation of Epac1 favors glucose metabolism and lactate production to supply rapidly energy ensuring cell survival. In addition, Epac1 promotes oxidation of fatty acids, lowers mitochondrial oxidative phosphorylation and enhances mitochondrial energy reserve. The involvement of Epac1 in metabolic events crucial for the preservation of structure and function of podocytes indicates the potential of Epac1 activation as an effective future treatment for glomerular diseases.

Disclosure Statement

All authors declared no competing interests

Author Contributions

L.A. and M.D. performed most of the experiments, analyzed data and participated in the writing of the manuscript;

P.K. and L.M. performed a part of the *in vivo* experiments;

T.M. and MC. V. performed glomeruli dissection and electron microscopy, respectively;

D.B, M.L and A.L performed cell culture, Seahorse analysis and immunoblot analysis.

C.C. and F.L designed and initiated the project, supervised the project and wrote the manuscript.

Funding

F.L. was supported by grants from Institut National de la Santé et de la Recherche Médicale, Université de Toulouse III-Paul Sabatier, the French National Agency for Research (ANR-17-CE14--0014-01, ANR-19-CE17-0010, Fondation pour la Recherche Médicale ("Equipes FRM 2021, EQU202103012601").

C.C. was supported by grants from the Institut National de la Santé et de la Recherche Médicale, Sorbonne Université, and the French National Agency for Research (ANR-17-CE14--0014-01).

Acknowledgements

We acknowledge the members of our laboratory for helpful suggestions and insights. We acknowledge members of the animal facilities of UMRS-U1155 CoRaKiD (Gaetan Girault and Liliane Louedec) and UMS-006 (UMS 006/INSERM/UPS, Anexplo/GenotoulPlateform)

for animal housing and care. We acknowledge the support from We-Met I2MC, GeT-Santé technical (Emeline Lhuillier) platform, IGenSeq and Data Analysis of Paris Brain Institute's-ICM, CoRaKiD platform of Histology (Souhila Ouchelouche). We thank Pr Moin Saleem, (Director of Bristol Renal) for the gift of the human podocyte cell line Ab8/13.

Data availability

RNAseq raw data have been deposited to GEO repository with accession number GSE237097 (as the data are private until publication, please find the token for reviewers: ezurcsgujbwjter.)

List of supplementary materials

- Supplementary Methods.
- Supplementary Figure S1. Renal goat and mouse IgG deposits in WT and Epac1$^{-/-}$ mice.
- Supplementary Figure S2. Co-immunostaining of Epac1 and CD44 in the renal cortex of Ctr and *Nphs2Cre*-Epac1$^{fl/fl}$ mice after NTS.
- Supplementary Figure S3. Transcriptomic signature in glomeruli underlying NTS-induced GN.
- Supplementary Figure S4. Transcriptomic signature of biological process in glomeruli underlying NTS-induced GN.
- Supplementary Figure S5. Transcriptomic signature of cellular compartment in glomeruli underlying NTS-induced GN.
- Supplementary Figure S6. Heatmap and Volcano plot of differentially expressed genes in glomeruli of Ctr NTS and *Nphs2Cre*-Epac1$^{fl/fl}$ mice at D4 and D11.
- Supplementary Figure S7. Epac1 inhibition dysregulates fatty acid pathway at the onset of GN.
- Supplementary Figure S8. Epac1 inhibition targets mitochondria at the onset of GN.

- Supplementary Figure S9. Epac1 drives a metabolic switch without affecting the number of mitochondria.
- Supplementary References.

References

1. Kazi, A. M. & Hashmi, M. F. Glomerulonephritis. in *Glomerulonephritis*. 2023.StatPearls Publishing.
2. Wetmore, J. B., Guo, H., Liu, J., Collins, A. J. & Gilbertson, D. T. The incidence, prevalence, and outcomes of glomerulonephritis derived from a large retrospective analysis. *Kidney Int.* 2016; 90: 853–860.
3. Halls, M. L. & Cooper, D. M. F. Adenylyl cyclase signalling complexes – Pharmacological challenges and opportunities. *Pharmacol. Ther*. 2017; 172: 171–180.
4. Beavo, J. A. & Brunton, L. L. Cyclic nucleotide research — still expanding after half a century. *Nat. Rev. Mol. Cell Biol.* 2002; 3: 710–717.
5. Sholokh, A. & Klussmann, E. Local cyclic adenosine monophosphate signalling cascades-Roles and targets in chronic kidney disease. *Acta Physiol.* 2021; 232: el3641.
6. De Rooij, J. *et al.* Epac is a Rap1 guanine-nucleotide-exchange factor directly activated by cyclic AMP. *Nature* 1998; 396: 474–477.
7. Kawasaki, H. *et al.* A Family of cAMP-Binding Proteins That Directly Activate Rap1. *Science*. 1998; 282: 2275–2279.
8. Formoso, K., Lezoualc'h, F. & Mialet-Perez, J. Role of EPAC1 Signalosomes in Cell Fate: Friends or Foes? *Cells*9. 2020; 1954.
9. Lezoualc'h, F., Fazal, L., Laudette, M. & Conte, C. Cyclic AMP Sensor EPAC Proteins and Their Role in Cardiovascular Function and Disease. *Circ. Res.* 2016; 118: 881–897.
10. Robichaux, W. G. & Cheng, X. Intracellular cAMP Sensor EPAC: Physiology, Pathophysiology, and Therapeutics Development. *Physiol. Rev.* 2018; 98: 919–1053.
11. Wang, Y. *et al.* Epac Regulates UT-A1 to Increase Urea Transport in Inner Medullary Collecting Ducts. *J. Am. Soc. Nephrol.* 2009; 20; 2018–2024.
12. Xie, P., Joladarashi, D., Dudeja, P., Sun, L. & Kanwar, Y. S. Modulation of angiotensin

II-induced inflammatory cytokines by the Epac1-Rap1A-NHE3 pathway: implications in renal tubular pathobiology. *Am. J. Physiol.-Ren. Physiol.* 2014; 306: F1260–F1274.

13. Cherezova, A. *et al.* Urinary concentrating defect in mice lacking Epac1 or Epac2. *FASEB J.* 2019; 33: 2156–2170.

14. Tomilin, V. N. *et al.*Epac1–/– and Epac2–/– mice exhibit deficient epithelial Na+ channel regulation and impaired urinary Na+ conservation. *JCI Insight*7. 2022; e145653.

15. Stokman, G. *et al.* Epac-Rap Signaling Reduces Cellular Stress and Ischemia-induced Kidney Failure. *J. Am. Soc. Nephrol.* 2011; 22: 859–872.

16. Stokman, G. *et al.* Epac-Rap Signaling Reduces Oxidative Stress in the Tubular Epithelium. *J. Am. Soc. Nephrol.* 2014; 25: 1474–1485.

17. Mesnard, L. *et al.* Invariant Natural Killer T Cells and TGF-β Attenuate Anti-GBM Glomerulonephritis. *J. Am. Soc. Nephrol.* 2009; 20: 1282–1292.

18. Salant, D. J. & Cybulsky, A. V. [38] Experimental glomerulonephritis. in vol. 1988, 162 421–461.

19. Kerroch, M. *et al.* Genetic inhibition of discoidin domain receptor 1 protects mice against crescentic glomerulonephritis. *FASEB J.* 2012; 26: 4079–4091.

20. Motonishi, S. *et al.* Sirtuin1 Maintains Actin Cytoskeleton by Deacetylation of Cortactin in Injured Podocytes. *J. Am. Soc. Nephrol.* 2015; 26: 1939–1959.

21. Laurent, A.-C. *et al.* Exchange protein directly activated by cAMP 1 promotes autophagy during cardiomyocyte hypertrophy. *Cardiovasc. Res.* 2015; 105: 55–64.

22. Susztak, K., Raff, A. C., Schiffer, M. & Böttinger, E. P. Glucose-Induced Reactive Oxygen Species Cause Apoptosis of Podocytes and Podocyte Depletion at the Onset of Diabetic Nephropathy. *Diabetes* 2006; 55: 225–233.

23. Audzeyenka, I., Bierżyńska, A. & Lay, A. C. Podocyte Bioenergetics in the

Development of Diabetic Nephropathy: The Role of Mitochondria. *Endocrinology*163, bqab234, 2022.

24. Marchetti, P., Fovez, Q., Germain, N., Khamari, R. & Kluza, J. Mitochondrial spare respiratory capacity: Mechanisms, regulation, and significance in non- transformed and cancer cells. *FASEB J.* 2020; 34: 13106–13124.

25. Ward, F., Holian, J. & Murray, P. T. Drug therapies to delay the progression of chronic kidney disease. *Clin. Med.* 2015: 15; 550–557.

26. Anders, H.-J., Kitching, A. R., Leung, N. & Romagnani, P. Glomerulonephritis: immunopathogenesis and immunotherapy. *Nat. Rev. Immunol.* 2023; 23: 453–471.

27. Yougbare, I., Keravis, T. & Lugnier, C. NCS 613, a PDE4 inhibitor, by increasing cAMP level suppresses systemic inflammation and immune complexes deposition in kidney of MRL/lpr lupus- prone mice. *Biochim. Biophys. Acta BBA - Mol. Basis Dis.* 2021; 1867: 166019.

28. Ding, H. *et al.* PDE/cAMP/Epac/C/EBP-β Signaling Cascade Regulates Mitochondria Biogenesis of Tubular Epithelial Cells in Renal Fibrosis. *Antioxid. Redox Signal.* 2018; 29: 637–652.

29. Fazal, L. *et al.* Multifunctional mitochondrial Epac1 controls myocardial cell death. *Circ. Res.* 2017; 120: 645–657.

30. Bouvet, Blondeau, & Lezoualc'h. The Epac1 Protein: Pharmacological Modulators, Cardiac Signalosome and Pathophysiology. *Cells*. 2019; 8: 1543.

31. Laudette, M. *et al.* Cyclic AMP-binding protein Epac1 acts as a metabolic sensor to promote cardiomyocyte lipotoxicity. *Cell Death Dis.* 2021; 12: 824.

32. Beeson, C. C., Beeson, G. C. & Schnellmann, R. G. A high-throughput respirometric assay for mitochondrial biogenesis and toxicity. *Anal. Biochem.* 2010; 404: 75–81.

33. Zheng, J. Energy metabolism of cancer: Glycolysis versus oxidative phosphorylation

(Review). *Oncol. Lett.* 2012; 4: 1151–1157.

34. Mirzaei, H. & Hamblin, M. R. Regulation of Glycolysis by Non-coding RNAs in Cancer: Switching on the Warburg Effect. *Mol. Ther. - Oncolytics*. 2020; 19: 218–239.

35. Ozawa, S. *et al.* Glycolysis, but not Mitochondria, responsible for intracellular ATP distribution in cortical area of podocytes. *Sci. Rep.* 2016; 5: 18575.

36. Brinkkoetter, P. T. *et al.* Anaerobic Glycolysis Maintains the Glomerular Filtration Barrier Independent of Mitochondrial Metabolism and Dynamics. *Cell Rep.* 2019; 27: 1551-1566.e5.

37. Yuan, Q. *et al.* Role of pyruvate kinase M2-mediated metabolic reprogramming during podocyte differentiation. *Cell Death Dis.* 2020;11: 355.

38. Fu, J. *et al.* Regeneration of glomerular metabolism and function by podocyte pyruvate kinase M2 in diabetic nephropathy. *JCI Insight*. 2022; e155260.

39. Zhang, Z. *et al.* PFKP Activation Ameliorates Foot Process Fusion in Podocytes in Diabetic Kidney Disease. *Front. Endocrinol.* 2022; 12: 797025.

40. Sieber, J. & Jehle, A. W. Free Fatty Acids and Their Metabolism Affect Function and Survival of Podocytes. *Front. Endocrinol.* 2014; 5: 186

41. Luengo, A. *et al.* Increased demand for NAD+ relative to ATP drives aerobic glycolysis. *Mol. Cell*. 2021; 8: 691-707.e6.

42. Granchi, C., Bertini, S., Macchia, M. & Minutolo, F. Inhibitors of Lactate Dehydrogenase Isoforms and their Therapeutic Potentials. *Curr. Med. Chem.* 2010; 17: 672–697.

43. Hui, S. *et al.* Glucose feeds the TCA cycle via circulating lactate. *Nature*. 2017; 551: 115–118.

44. Li, X. *et al.* Lactate metabolism in human health and disease. *Signal Transduct. Target. Ther.* 2022; 7: 305.

45. Rabinowitz, J. D. & Enerbäck, S. Lactate: the ugly duckling of energy metabolism. *Nat. Metab.* 2020; 2: 566–571.

46. Warburg, O. The Metabolism of Carcinoma Cells. *J. Cancer Res.* 1925; 9: 148–163.

47. Atlante, A. *et al*. A disease with a sweet tooth: exploring the Warburg effect in Alzheimer's disease. *Biogerontology*. 2017; 18, 301–319.

48. Gambardella, J. *et al*. Experimental evidence and clinical implications of Warburg effect in the skeletal muscle of Fabry disease. *iScience*. 2023; 26, 106074.

49. Shimada, S. *et al.*Metabolic responses of normal rat kidneys to a high salt intake. *BioRxiv*. 2023; 524636.

Figure Legends

Figure 1. Epac1 deletion accelerates progression of renal disease after NTS-induced GN.

(**a**) Representative Western blots from whole kidney lysates of WT and Epac1$^{-/-}$ mice. (**b**) Expression of Epac1 in renal cortex. Scale bars are 20 µM. (**c**) Flow chart of the protocol: WT and Epac1$^{-/-}$ mice are treated with 2 consecutive injections of NTS or PBS and followed until day 15. Proteinuria (**d**) and plasma urea (**e**) are increased in Epac1$^{-/-}$ mice following NTS. (**f**) mRNA expression of markers of fibrosis (Col I), inflammation (VCAM-1, MCP-1) and kidney injury (NGAL). Statistical analysis was performed using one-way ANOVA, or two-way ANOVA for proteinuria. $^{\#}P<0.05$, $^{\#\#\#}P<0.001$, $^{\#\#\#\#}P<0.0001$ versus baseline; $^{*}P<0.05$, $^{**}P<0.01$, $^{***}P<0.001$ versus WT mice injected with NTS, n=6-7 per group

Figure 2. Epac1 deletion aggravates renal damage and fibrosis in GN.

Protein expression of Col I, α-SMA and KIM-1 are enhanced in kidneys of Epac1$^{-/-}$ mice after NTS. Scale bars are 50 µM. Statistical analysis was performed using one-way ANOVA. $^{\#}P<0.05$, $^{\#\#}P<0.01$, $^{\#\#\#}P<0.001$, $^{\#\#\#\#}P<0.0001$ versus baseline; $^{*}P<0.05$, $^{**}P<0.01$ versus WT mice injected with NTS, n=6-7 per group.

Figure 3. Epac1 deletion promotes crescents formation, inflammation and podocytes injury

Morphological and immuno-histological analysis of kidney sections with quantification (bottom) illustrating the deterioration of the renal structure in Epac1$^{-/-}$ mice. Left column represents staining showing fibrosis and crescent formation (black arrows) after NTS treatment. Crescent quantification is expressed as the percentage of glomeruli presenting crescents. Middle panels show renal macrophages assessed by F4/80 staining. Right column represents immunofluorescence staining of WT-1; results are expressed as positive number

for WT-1 staining nuclei per glomerulus. Scale bars are 50 µM, 100 µM and 20 µM, respectively. Individual values are shown along with group mean ± SEM for WT and Epac1$^{-/-}$ mice without and after NTS administration. Statistical analysis was performed using one-way ANOVA. $^{\#}P<0.05$, $^{\#\#\#}P<0.001$, $^{\#\#\#\#}P<0.0001$ versus baseline; $^{*}P<0.05$, $^{**}P<0.01$, $^{***}P<0.001$ versus WT mice injected with NTS, n=6-7 per group.

Figure 4. Podocyte-specific deletion of Epac1 aggravates the development of NTS-induced GN.

(**a**) Dual immunolabeling of Epac1 (green) and the podocyte marker nestin (red) on kidneys from control (Ctr) and conditional mice (*Nphs2Cre*-Epac1$^{fl/fl}$) with the corresponding quantification (right) Scale bars are 20 µM. (**b**) Flow chart of the protocol: mice are treated with 2 consecutive injections of NTS or PBS and followed until day 15. Renal function evaluated by (**c**) proteinuria, (**d**) plasma urea and (**e**) plasma creatinine concentrations. Statistical analysis was performed using one-way ANOVA, or two-way ANOVA for proteinuria; $^{\#}P<0.05$, $^{\#\#\#}P<0.001$, $^{\#\#\#\#}P<0.0001$versus baseline; $^{*}P<0.05$, $^{**}P<0.01$, $^{***}P<0.001$ versus Ctr mice injected with NTS.

Figure 5. Podocyte-specific deletion of Epac1 promotes renal damage and fibrosis in NTS-induced GN.

(**a**) mRNA and (**b**) protein expression of markers of fibrosis, renal damage and inflammation Col I, KIM-1, VCAM-1, MCP-1 and NGAL in whole kidney samples. Scale bars are 50 µM. Individual values are shown along with group mean ± SEM for Ctr PBS, *Nphs2Cre*-Epac1$^{fl/fl}$ PBS, Ctr NTS, and *Nphs2Cre*-Epac1$^{fl/fl}$ NTS (n=6 per group). Statistical analysis was performed using one-way ANOVA; $^{\#}P<0.05$, $^{\#\#\#}P<0.001$, $^{\#\#\#\#}P<0.0001$versus baseline; $^{*}P<0.05$, $^{**}P<0.01$ versus Ctr mice injected with NTS.

Figure 6. Podocyte-specific deletion of Epac1 enhances crescent formation, inflammatory infiltration and podocytes alteration in GN.

Morphological and immuno-histological analysis of kidney sections (top) with quantification (bottom) illustrating the deterioration of the renal structure in *Nphs2Cre*-Epac1$^{fl/fl}$ mice. Representative images of Trichrome Masson's staining (left) with glomerular crescents quantification, inflammatory macrophages infiltration (middle) revealed by F4/80 staining, and ultrastructure analysis of glomeruli by transmission electronic microscopy (TEM, right). Scale bars are 50 µM, 100 µM and 2µM, respectively. Individual values are shown along with group mean ± SEM for Ctr PBS, *Nphs2Cre*-Epac1$^{fl/fl}$ PBS, Ctr NTS, and *Nphs2Cre*-Epac1$^{fl/fl}$ NTS (n=6 per group) except for TEM (n=3 per group). Statistical analysis was performed using one-way ANOVA; $^{\#}P<0.05$, $^{\#\#}P<0.01$, $^{\#\#\#\#}P<0.0001$versus baseline; $^{***}P<0.001$ versus Ctr mice injected with NTS.

Figure 7. Epac1 inhibition targets metabolic processes at the onset of GN progression. (**a**) Flow chart of the RNA sequencing with the RNA extraction from the glomeruli at day 4 and 11 after NTS induction. (**b**) Enrichment analysis of biological process gene ontology terms for differentially regulated genes on D4 and (**c**) D11. Up-regulated and down-regulated processes in Ctr NTS vs. *Nphs2Cre*-Epac1$^{fl/fl}$ NTS are represented in red and blue, respectively.

Figure 8. Epac1 inhibition dysregulates glycolysis and oxidative phosphorylation pathways.

(**a**) Heatmap showing differentially regulated genes between Ctr NTS and *Nphs2Cre*-Epac1$^{fl/fl}$ NTS related to the glycolysis on D4 and (**b**) related to the oxidative phosphorylation

at D11 (FDR < 0.05). Up-regulated and down-regulated genes in Ctr NTS vs. *Nphs2Cre-Epac1*$^{fl/fl}$ NTS are represented in red and blue, respectively.

Figure 9. Epac1 improves mitochondrial function.

(**a**) Cell viability H_2O_2 (200 µM) treatment for 6 hours, 8-CPT-AM (10 µM) is added 30 min before and during the H_2O_2 treatment (n=6 biological replicates). (**b**) Podocyte migration expressed as percentage of wound closure over 24 h (H_2O_2: 200 µM; 8-CPT-AM: 10 µM) (n=83-85 images from 7 independent experiments). (**c**) Representative images of the scratch test. (**d**) Profile of the seahorse oxygen consumption rate (OCR) with Cell Mito Stress Test. H_2O_2 (150 µM) treatment for 4 hours, 8-CPT-AM (10 µM) is added 30 min before and during the H_2O_2 treatment. Then seahorse tests are performed. Oligomycin (1 µM) inhibits ATP synthase. FCCP (4 µM) uncouples the H+ of the inter membrane space. Rotenone (1 µM) and antimycine A (1 µM) inhibit the complex I & III (n=14-17 biological replicates). (**e**) Baseline OCR (basal OCR – minimum OCR after ROT/AA). (**f**) ATP production OCR (Baseline OCR – after oligomycin OCR). (**g**) Spare respiratory capacity (maximum OCR after FCCP – Baseline OCR) a reflect of the mitochondrial respiration reserve (mitochondrial complexes efficacy, substrates availability and oxidation abilities). (**h**) Proton leak (after oligomycin OCR - minimum OCR after ROT/AA) uncouples the H^+ gradient those H^+ will not participate to ATP production. If normality is respected, one-way ANOVA followed by Tukey test is performed, if not, Kruskall Wallis test followed by Dunn's test is done. **P*<0.05, ***P*<0.01, ****P*<0.001, *****P*<0.0001.

Figure 10. Epac1 promotes aerobic glycolysis to protect podocytes from oxidative stress injury.

(**A**) Profile of the Seahorse extracellular acidification rate (ECAR) with the Glycolysis Stress Test. H_2O_2 (150 µM) treatment for 4 hours, 8-CPT-AM (10 µM) is added 30 min before and during the H_2O_2 treatment. The assay medium is depleted in glucose, then saturating concentration of glucose (10 mM) is added followed by oligomycin (1 µM) and 2-Deoxy-d-glucose (2-DG, 50 mM) (n=18-23 biological replicates). (**B**) Basal glycolysis (after glucose injection ECAR - glucose starved medium ECAR). (**C**) Glucose dependency, with the Seahorse Mito Fuel Flex test, is the percentage of OCR related to glucose oxidation in the mitochondria (mitochondrial pyruvate carrier inhibition with UK-5099; 2 µM). Total OCR inhibition is measured with glutamate and palmitate oxidation inhibition (BPTES, allosteric inhibitor of glutaminase converting glutamine to glutamate, 3 µM; and Etomoxir inhibits carnitine palmitoyl-transferase 1A, 4 µM), (n=18-23 biological replicates). (**D**) Lactate concentration of cell supernatants (n=5 biological replicates). (**E**) Cell viability (n=6 biological replicates); H_2O_2 (200 µM) treatment for 6 hours, 8-CPT-AM (10 µM) is added 30 min before and during the H_2O_2 treatment, 2-DG (10 mM). (**F**) Podocyte migration expressed as percentage of wound closure over 24 h (H_2O_2: 200 µM; 8-CPT-AM:10 µM; 2-DG: 50 mM; sodium pyruvate: 1 mM) (n=83-89 images from 7 independent experiments). If normality is respected, one-way ANOVA followed by Tukey test is performed, if not, Kruskal-Wallis test followed by Dunn's test is done. **P*<0.05, ***P*<0.01, ****P*<0.001, *****P*<0.0001. (**G**) Schematic representation concluding our findings of Epac1 activation on podocytes under oxidative stress. In the cytosol, Epac1 enhances glycolysis to produce pyruvate which is subsequently converted to lactate. In mitochondria, Epac1 increases mitochondrial reserve, decreases mitochondrial respiration and promotes oxidation of fatty acids. The final outcome is improvement of podocyte viability. (Created with BioRender.com).

Figure 11. Epac1 pharmacological activation delays NTS-induced GN progression.

(**a**) Schematic representation of the protocol: following injections of NTS or PBS for 2 consecutive days, the Epac1 agonist 8-pCPT or vehicle (PBS) was continuously administered subcutaneously from day 3 to day 15 using an osmotic minipump in WT mice. Renal function evaluated by (**b**) proteinuria and (**c**) plasma creatinine concentration. (**d**) Representative images of Trichrome Masson's (left) with glomerular crescents (black arrows), macrophages/monocytes F4/80 immunohistochemistry (middle) and WT-1 immunofluorescence (right) staining with the corresponding quantification (bottom). Scale bars are 50 µM, 100 µM and 20 µM, respectively. Individual values are shown along with group mean ± SEM for WT PBS, 8-pCPT PBS, WT NTS and 8-pCPT NTS. Statistical analysis was performed using one-way ANOVA, or two-way ANOVA for proteinuria. $^{\#}P<0.05$, $^{\#\#}P<0.01$, $^{\#\#\#}P<0.001$, $^{\#\#\#\#}P<0.0001$ versus baseline; $^{*}P<0.05$, $^{**}P<0.01$, $^{***}P<0.001$ versus WT mice injected with NTS, n=6 per group.

Figure 12. Mice lacking Epac1 expression in podocytes are not protected against GN by pharmacological activation of Epac1.

(**a**) Schematic representation of the protocol: following injections of NTS or PBS for 2 consecutive days, the Epac1 agonist 8-pCPT or vehicle (PBS) was continuously administered subcutaneously starting from day 3 to day 15 using an osmotic minipump in *Nphs2Cre-*Epac1$^{fl/fl}$ and Ctr mice. Renal function evaluated by (**b**) proteinuria, (**c**) plasma urea and (**d**) plasma creatinine concentrations. (**e**) Representative images of Trichrome Masson's with the corresponding quantification of crescents (left). Scale bars are 20 µM. Statistical analysis was performed using one-way ANOVA, or two-way ANOVA for proteinuria. $^{\#}P<0.05$, $^{\#\#}P<0.01$, $^{\#\#\#}P<0.001$, $^{\#\#\#\#}P<0.0001$ versus baseline.

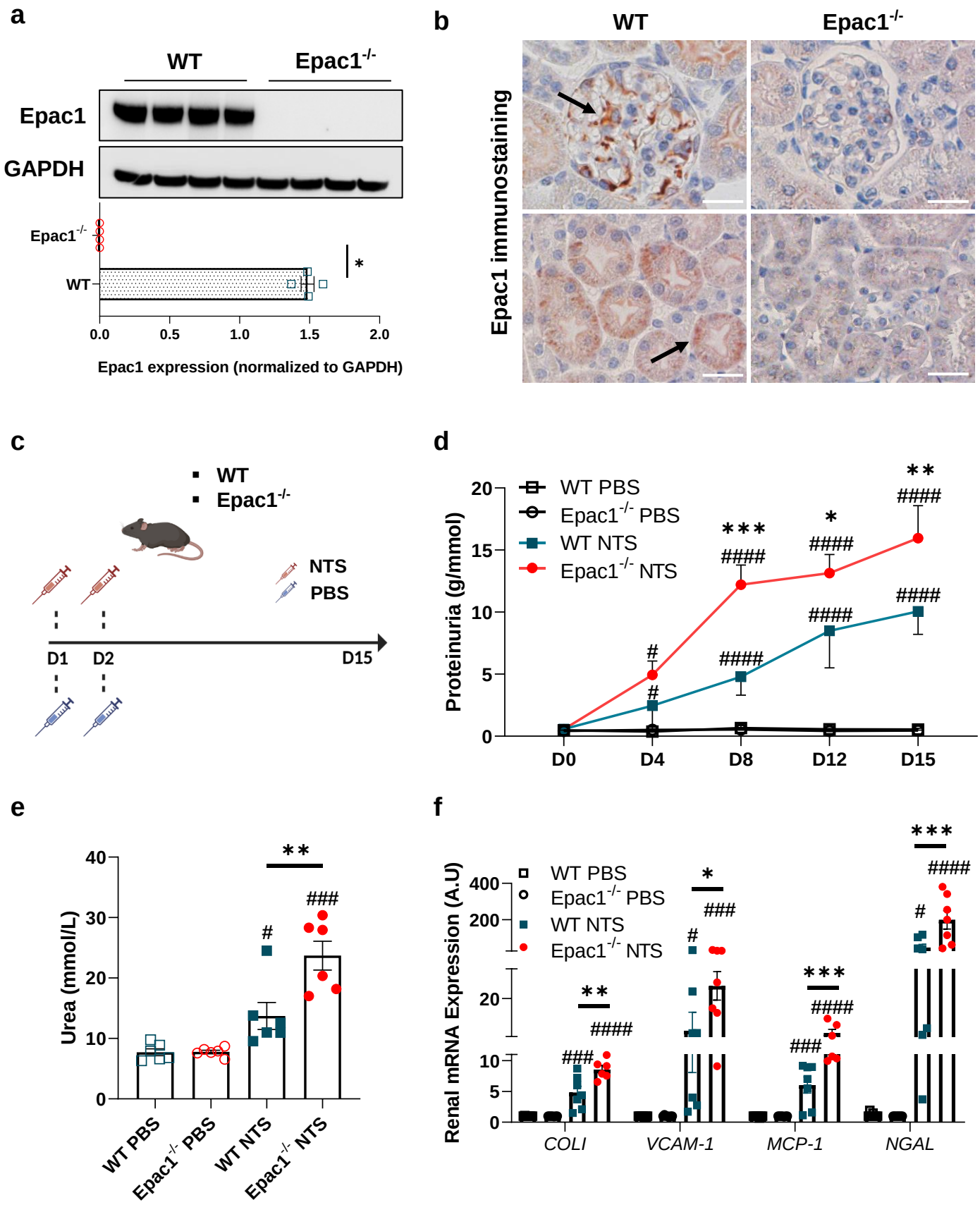
a
WT
Epac1-/-
Epac1
GAPDH
Epac1-/-
WT
*
0.0
0.5
1.0
1.5
2.0
Epac1 expression (normalized to GAPDH)
b
WT
Epac1-/-
Epac1 immunostaining
c
WT
Epac1-/-
NTS
PBS
D1
D2
D15
d
WT PBS
Epac1-/- PBS
WT NTS
Epac1-/- NTS
Proteinuria (g/mmol)
20
15
10
5
0
D0
D4
D8
D12
D15
**
####
***
####
*
####
#
#
####
####
####
e
Urea (mmol/L)
40
30
20
10
0
**
###
#
WT PBS
Epac1-/- PBS
WT NTS
Epac1-/- NTS
f
WT PBS
Epac1-/- PBS
WT NTS
Epac1-/- NTS
Renal mRNA Expression (A.U)
400
200
20
10
5
0
**
####
###
*
###
#
***
####
###
***
####
#
COLI
VCAM-1
MCP-1
NGAL

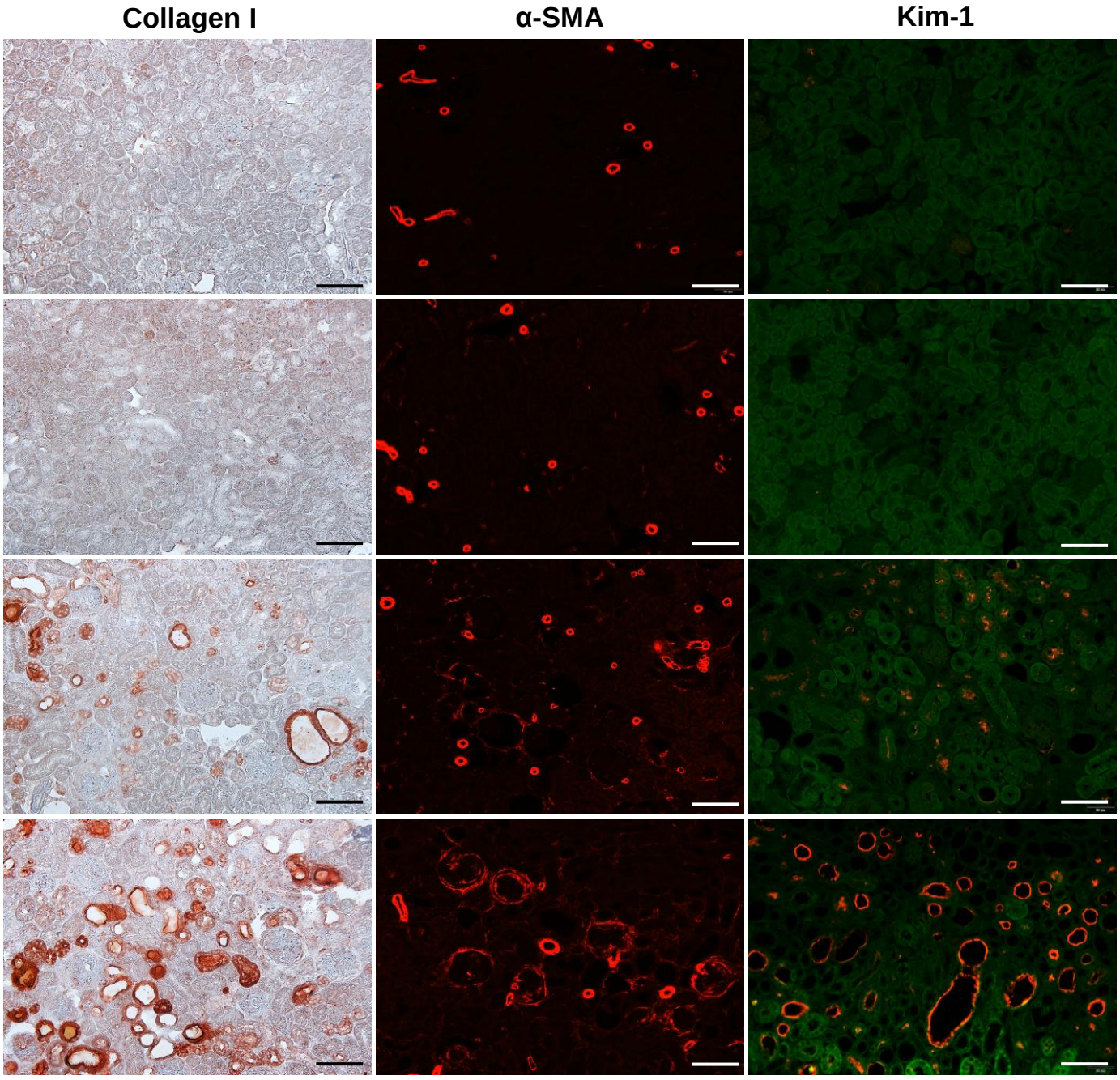
Collagen I
α-SMA
Kim-1
WT PBS
EPAC1-/- PBS
WT NTS
EPAC1-/- NTS

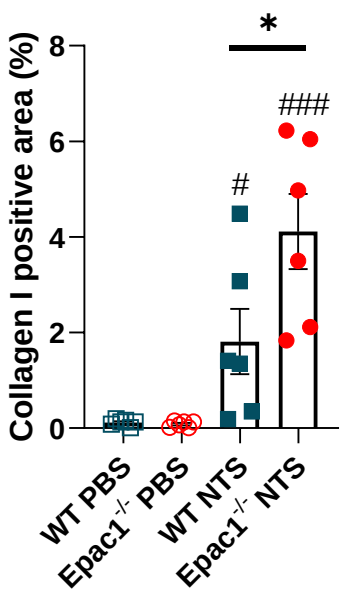
Collagen I positive area (%)
0
2
4
6
8
*
#
###
WT PBS
Epac1-/- PBS
WT NTS
Epac1-/- NTS

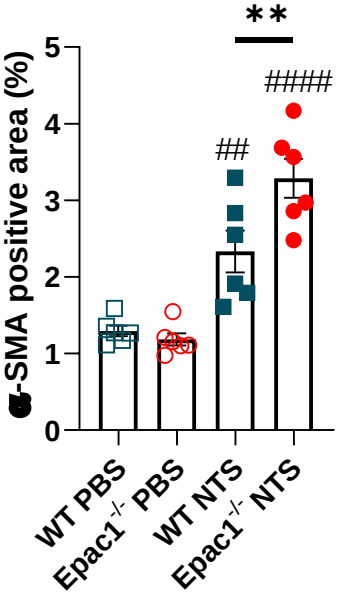
α-SMA positive area (%)
0
1
2
3
4
5
**
##
####
WT PBS
Epac1-/- PBS
WT NTS
Epac1-/- NTS

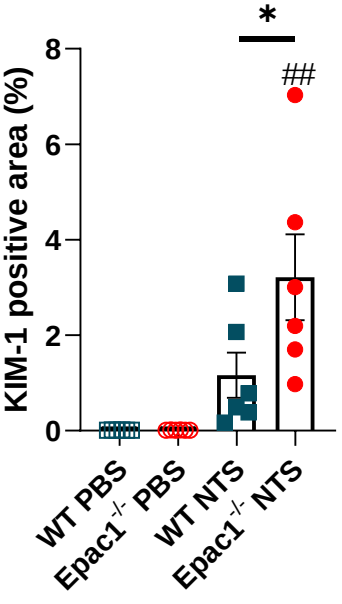
KIM-1 positive area (%)
0
2
4
6
8
*
##
WT PBS
Epac1-/- PBS
WT NTS
Epac1-/- NTS

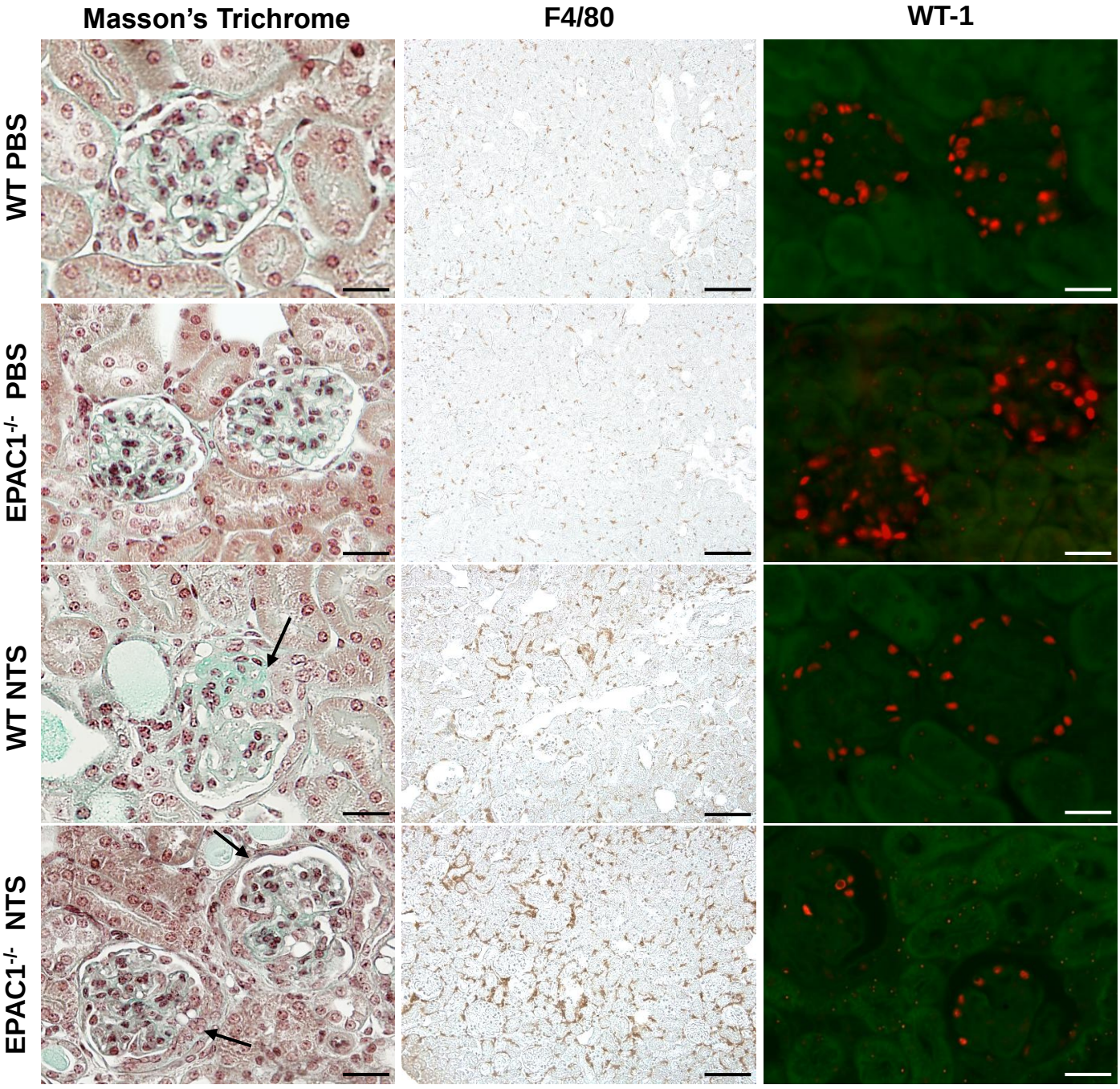
Masson's Trichrome
F4/80
WT-1
WT PBS
EPAC1-/- PBS
WT NTS
EPAC1-/- NTS

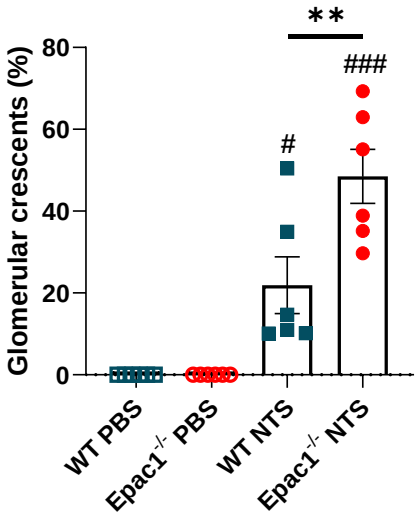
Glomerular crescents (%)
0
20
40
60
80
**
###
#
WT PBS
Epac1-/- PBS
WT NTS
Epac1-/- NTS

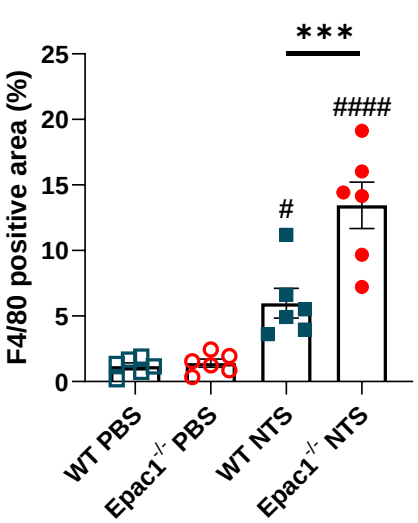
F4/80 positive area (%)
0
5
10
15
20
25
***
####
#
WT PBS
Epac1-/- PBS
WT NTS
Epac1-/- NTS

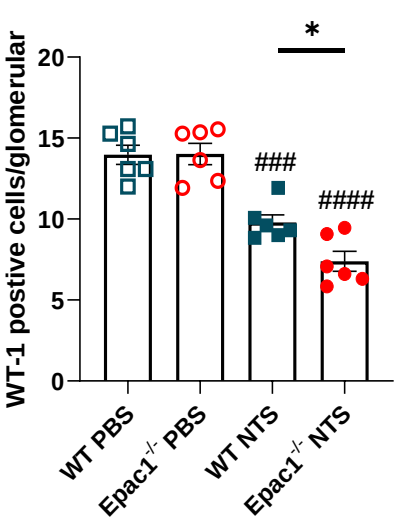
WT-1 postive cells/glomerular
0
5
10
15
20
*
###
####
WT PBS
Epac1-/- PBS
WT NTS
Epac1-/- NTS

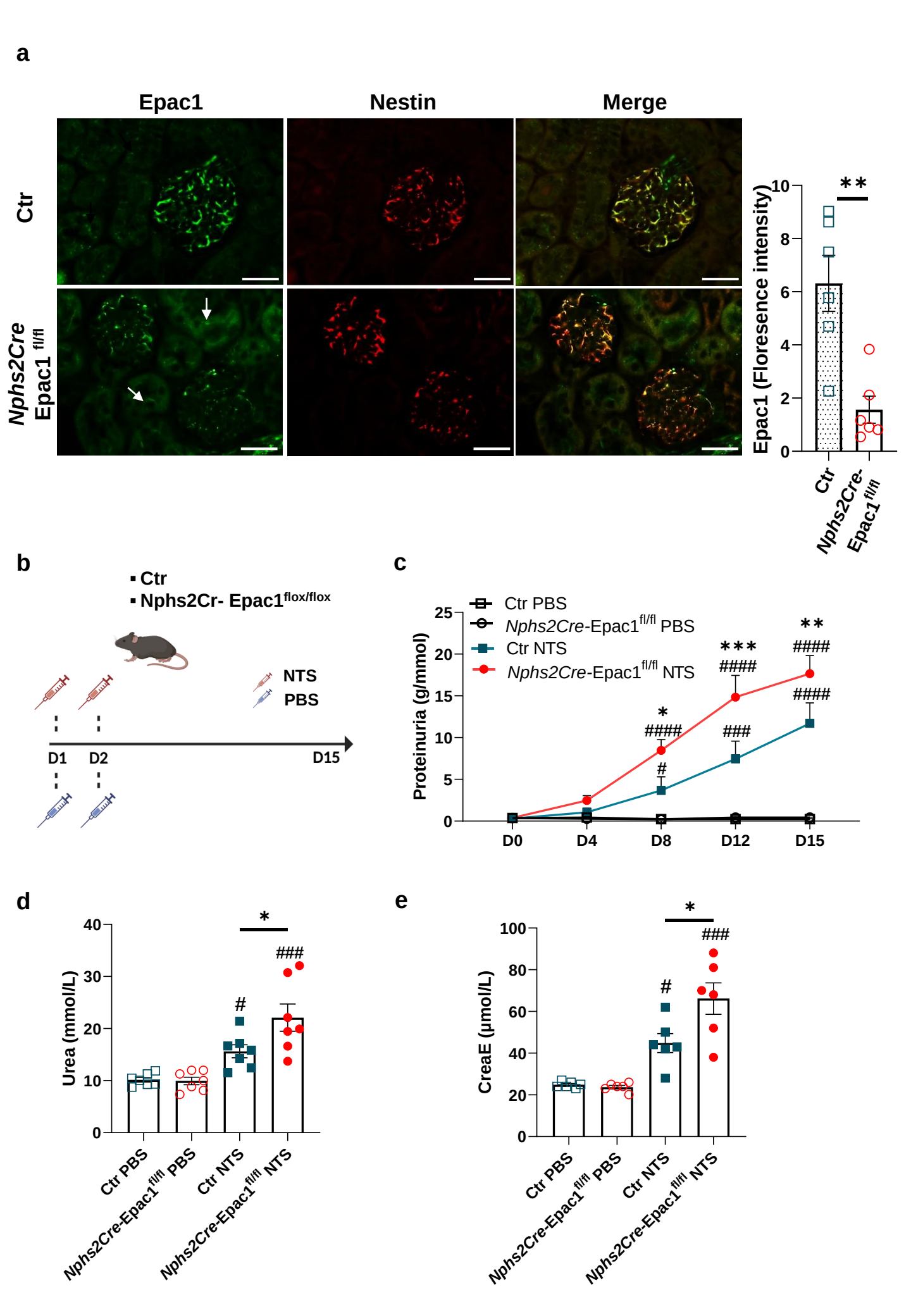
a
Epac1
Nestin
Merge
Ctr
Nphs2Cre Epac1 fl/fl
Epac1 (Floresence intensity)
**
Ctr
Nphs2Cre-Epac1 fl/fl
b
Ctr
Nphs2Cr- Epac1flox/flox
NTS
PBS
D1
D2
D15
c
Ctr PBS
Nphs2Cre-Epac1 fl/fl PBS
Ctr NTS
Nphs2Cre-Epac1 fl/fl NTS
Proteinuria (g/mmol)
D0
D4
D8
D12
D15
d
Urea (mmol/L)
Ctr PBS
Nphs2Cre-Epac1 fl/fl PBS
Ctr NTS
Nphs2Cre-Epac1 fl/fl NTS
e
CreaE (µmol/L)
Ctr PBS
Nphs2Cre-Epac1 fl/fl PBS
Ctr NTS
Nphs2Cre-Epac1 fl/fl NTS

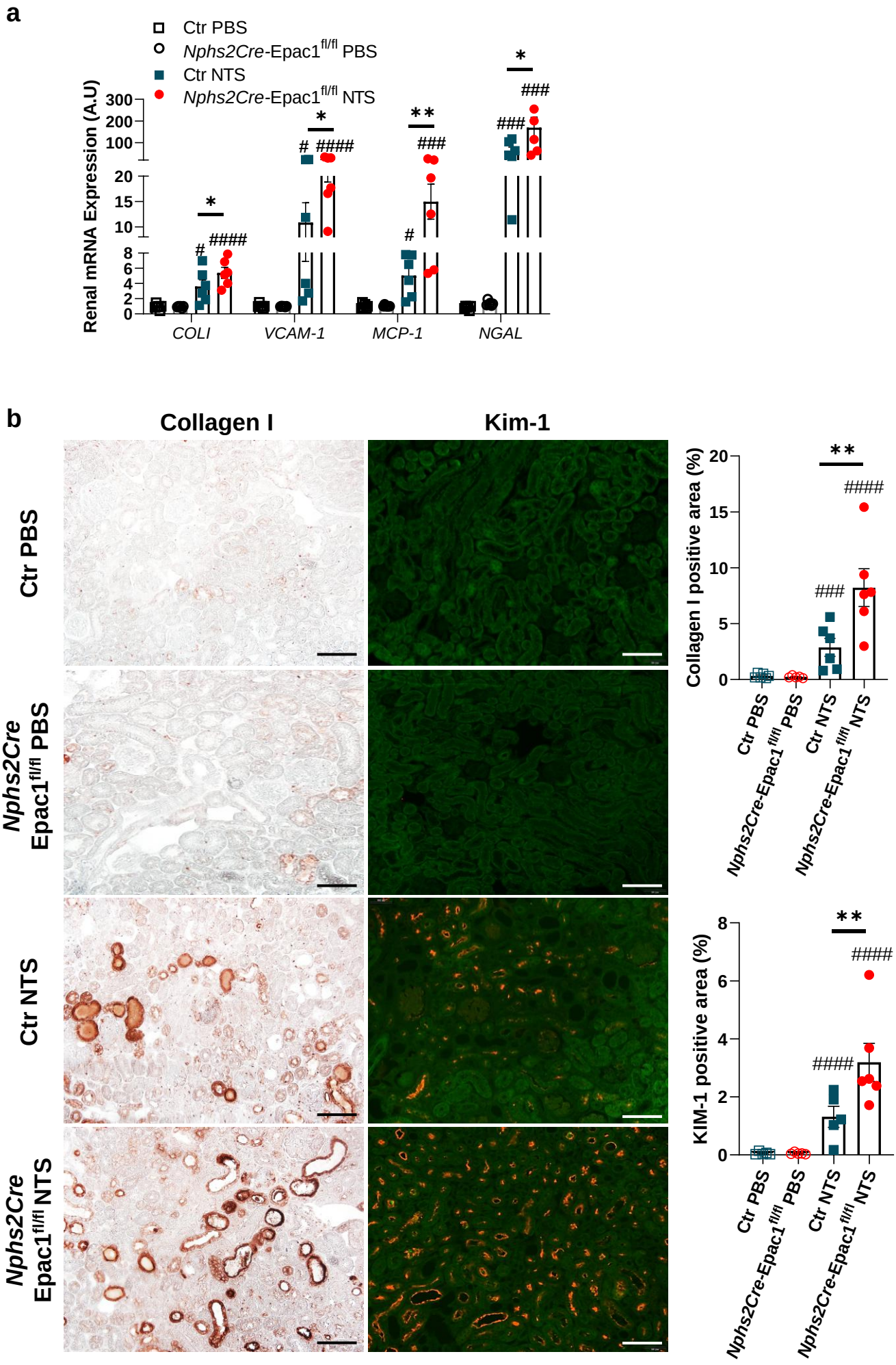
a
Ctr PBS
Nphs2Cre-Epac1fl/fl PBS
Ctr NTS
Nphs2Cre-Epac1fl/fl NTS
Renal mRNA Expression (A.U)
COLI
VCAM-1
MCP-1
NGAL
b
Collagen I
Kim-1
Ctr PBS
Nphs2Cre Epac1fl/fl PBS
Ctr NTS
Nphs2Cre Epac1fl/fl NTS
Collagen I positive area (%)
KIM-1 positive area (%)

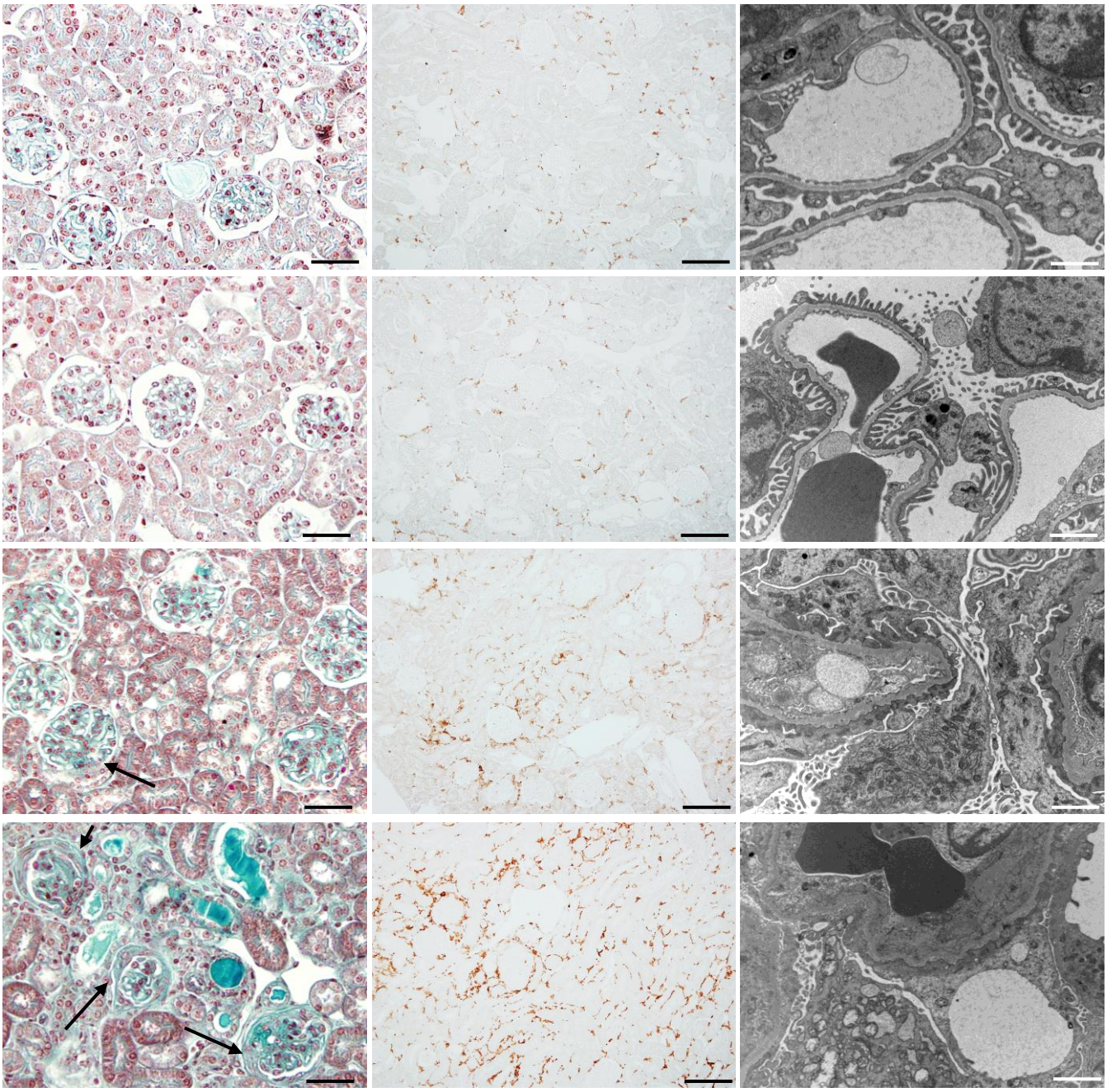
Masson's Trichrome
F4/80
TEM
Ctr PBS
Nphs2Cre Epac1fl/fl PBS
Ctr NTS
Nphs2Cre Epac1fl/fl NTS

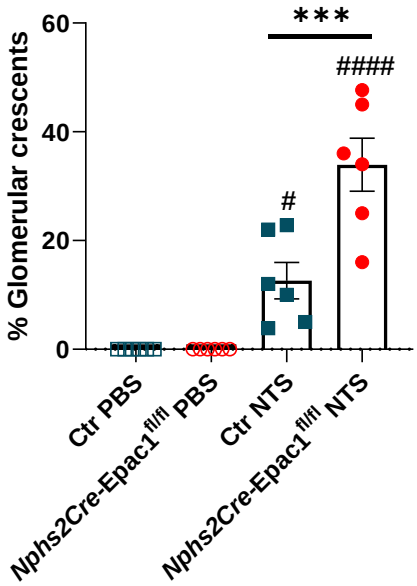
% Glomerular crescents
60
40
20
0
***
####
#
Ctr PBS
Nphs2Cre-Epac1fl/fl PBS
Ctr NTS
Nphs2Cre-Epac1fl/fl NTS

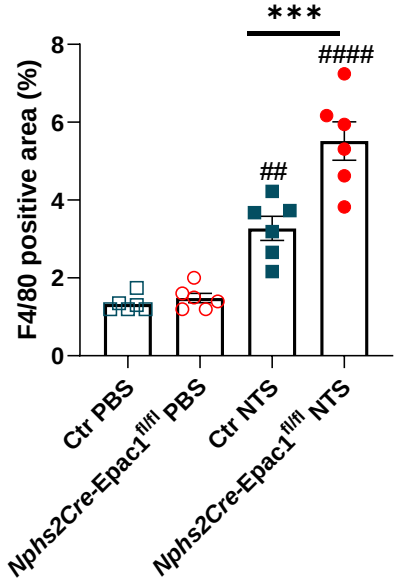
F4/80 positive area (%)
8
6
4
2
0
***
####
##
Ctr PBS
Nphs2Cre-Epac1fl/fl PBS
Ctr NTS
Nphs2Cre-Epac1fl/fl NTS

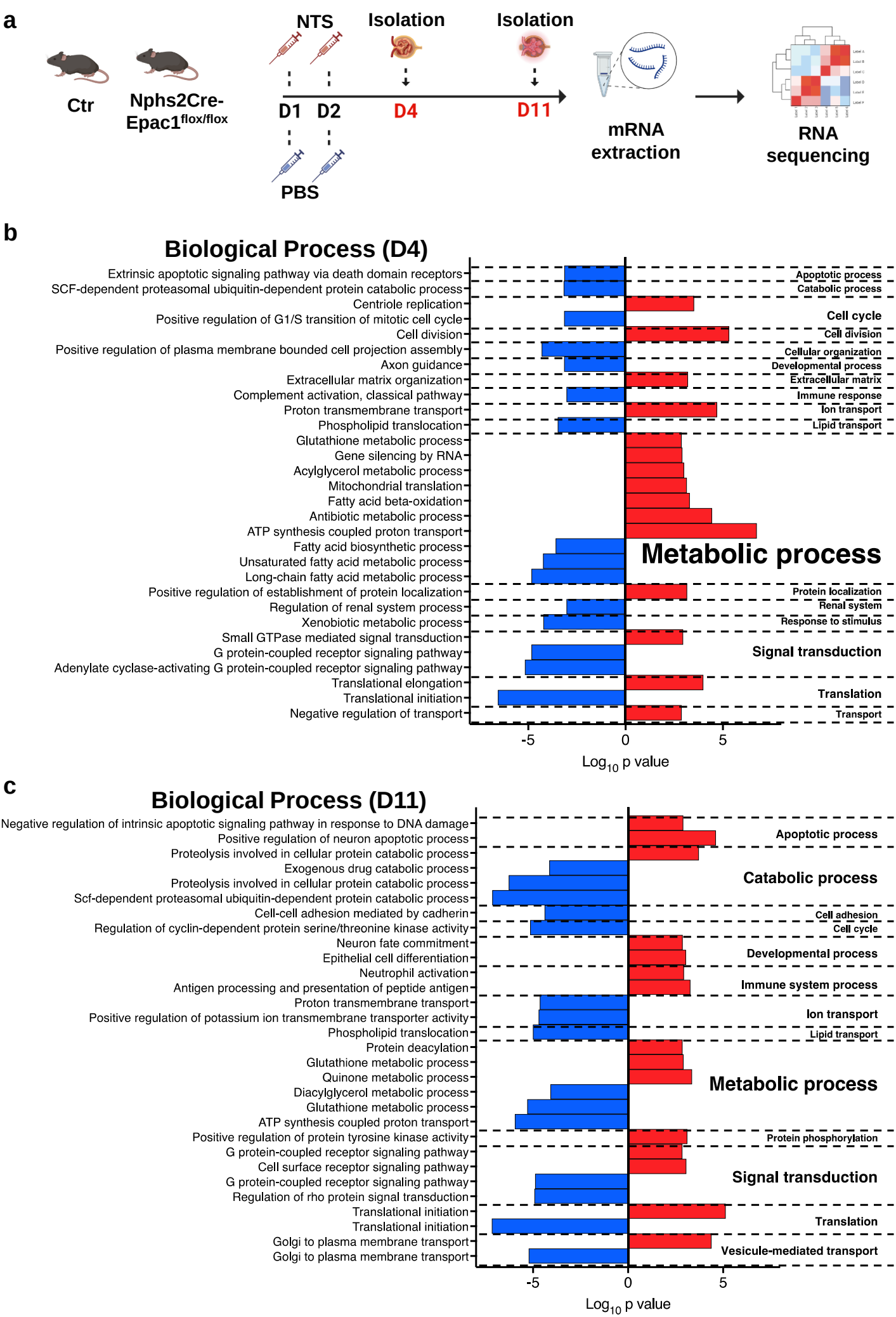
a
Ctr
Nphs2Cre-Epac1flox/flox
NTS
Isolation
Isolation
D1
D2
D4
D11
PBS
mRNA extraction
RNA sequencing
b
Biological Process (D4)
Extrinsic apoptotic signaling pathway via death domain receptors
SCF-dependent proteasomal ubiquitin-dependent protein catabolic process
Centriole replication
Positive regulation of G1/S transition of mitotic cell cycle
Cell division
Positive regulation of plasma membrane bounded cell projection assembly
Axon guidance
Extracellular matrix organization
Complement activation, classical pathway
Proton transmembrane transport
Phospholipid translocation
Glutathione metabolic process
Gene silencing by RNA
Acylglycerol metabolic process
Mitochondrial translation
Fatty acid beta-oxidation
Antibiotic metabolic process
ATP synthesis coupled proton transport
Fatty acid biosynthetic process
Unsaturated fatty acid metabolic process
Long-chain fatty acid metabolic process
Positive regulation of establishment of protein localization
Regulation of renal system process
Xenobiotic metabolic process
Small GTPase mediated signal transduction
G protein-coupled receptor signaling pathway
Adenylate cyclase-activating G protein-coupled receptor signaling pathway
Translational elongation
Translational initiation
Negative regulation of transport
Apoptotic process
Catabolic process
Cell cycle
Cell division
Cellular organization
Developmental process
Extracellular matrix
Immune response
Ion transport
Lipid transport
Metabolic process
Protein localization
Renal system
Response to stimulus
Signal transduction
Translation
Transport
-5
0
5
Log10 p value
c
Biological Process (D11)
Negative regulation of intrinsic apoptotic signaling pathway in response to DNA damage
Positive regulation of neuron apoptotic process
Proteolysis involved in cellular protein catabolic process
Exogenous drug catabolic process
Proteolysis involved in cellular protein catabolic process
Scf-dependent proteasomal ubiquitin-dependent protein catabolic process
Cell-cell adhesion mediated by cadherin
Regulation of cyclin-dependent protein serine/threonine kinase activity
Neuron fate commitment
Epithelial cell differentiation
Neutrophil activation
Antigen processing and presentation of peptide antigen
Proton transmembrane transport
Positive regulation of potassium ion transmembrane transporter activity
Phospholipid translocation
Protein deacylation
Glutathione metabolic process
Quinone metabolic process
Diacylglycerol metabolic process
Glutathione metabolic process
ATP synthesis coupled proton transport
Positive regulation of protein tyrosine kinase activity
G protein-coupled receptor signaling pathway
Cell surface receptor signaling pathway
G protein-coupled receptor signaling pathway
Regulation of rho protein signal transduction
Translational initiation
Translational initiation
Golgi to plasma membrane transport
Golgi to plasma membrane transport
Apoptotic process
Catabolic process
Cell adhesion
Cell cycle
Developmental process
Immune system process
Ion transport
Lipid transport
Metabolic process
Protein phosphorylation
Signal transduction
Translation
Vesicule-mediated transport
-5
0
5
Log10 p value

a

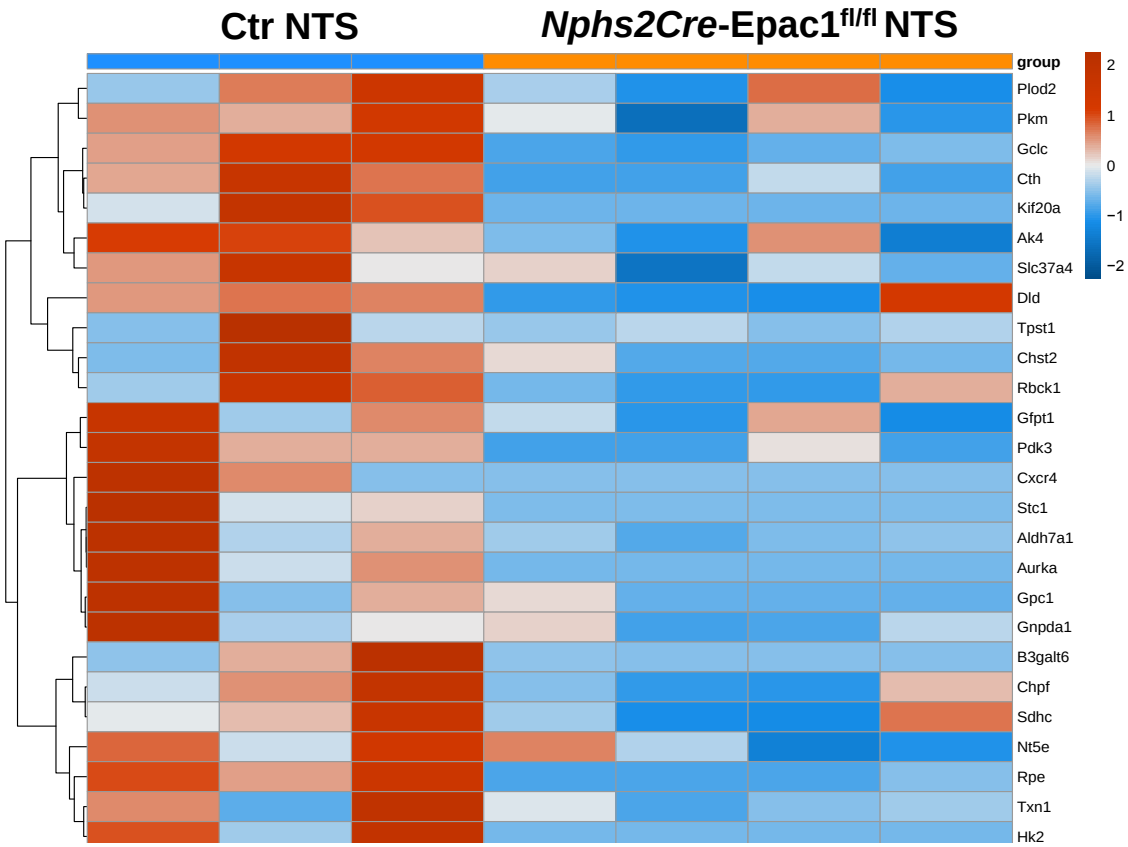

D4:Hallmark Glycolysis

b

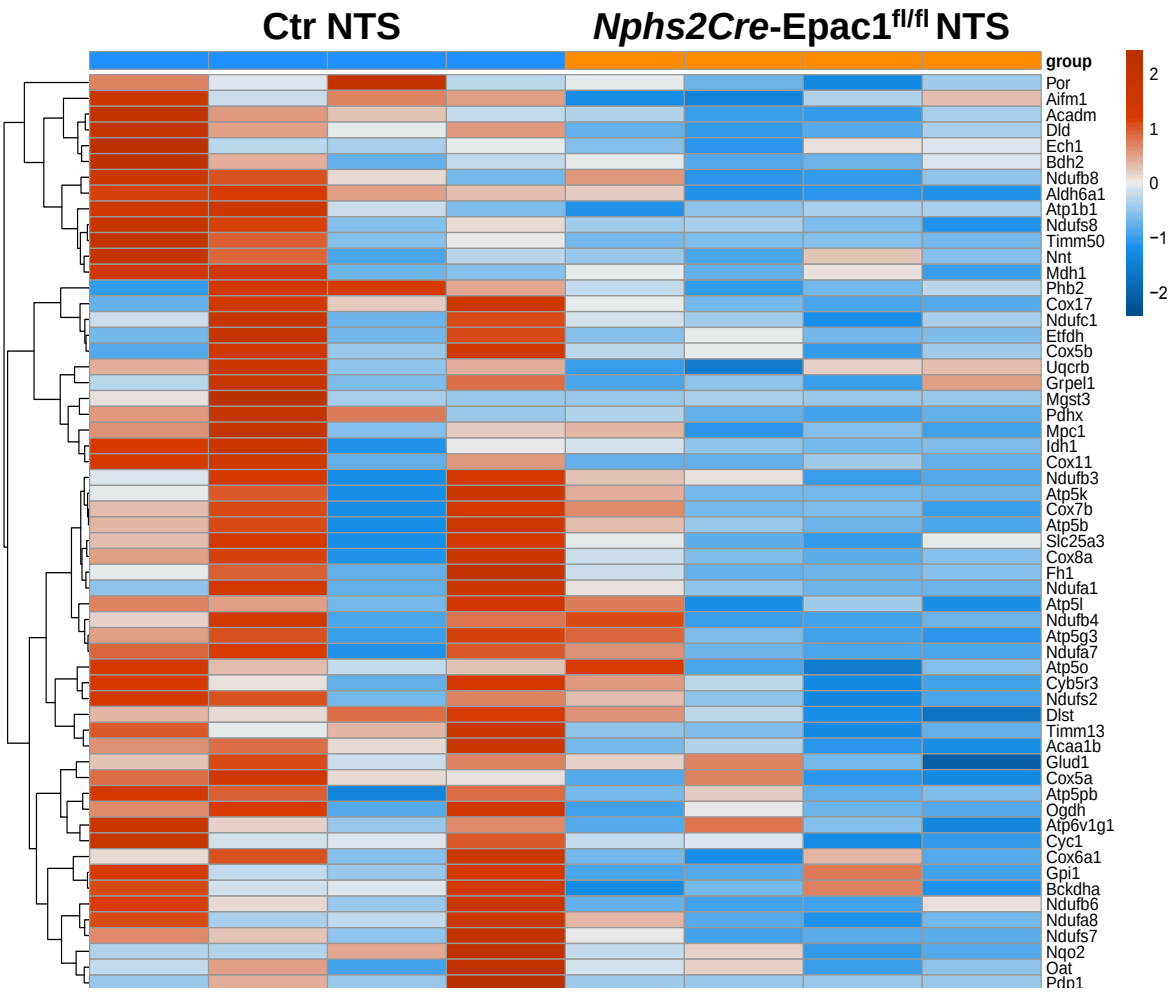

D11:Hallmark Oxidative Phosphorylation

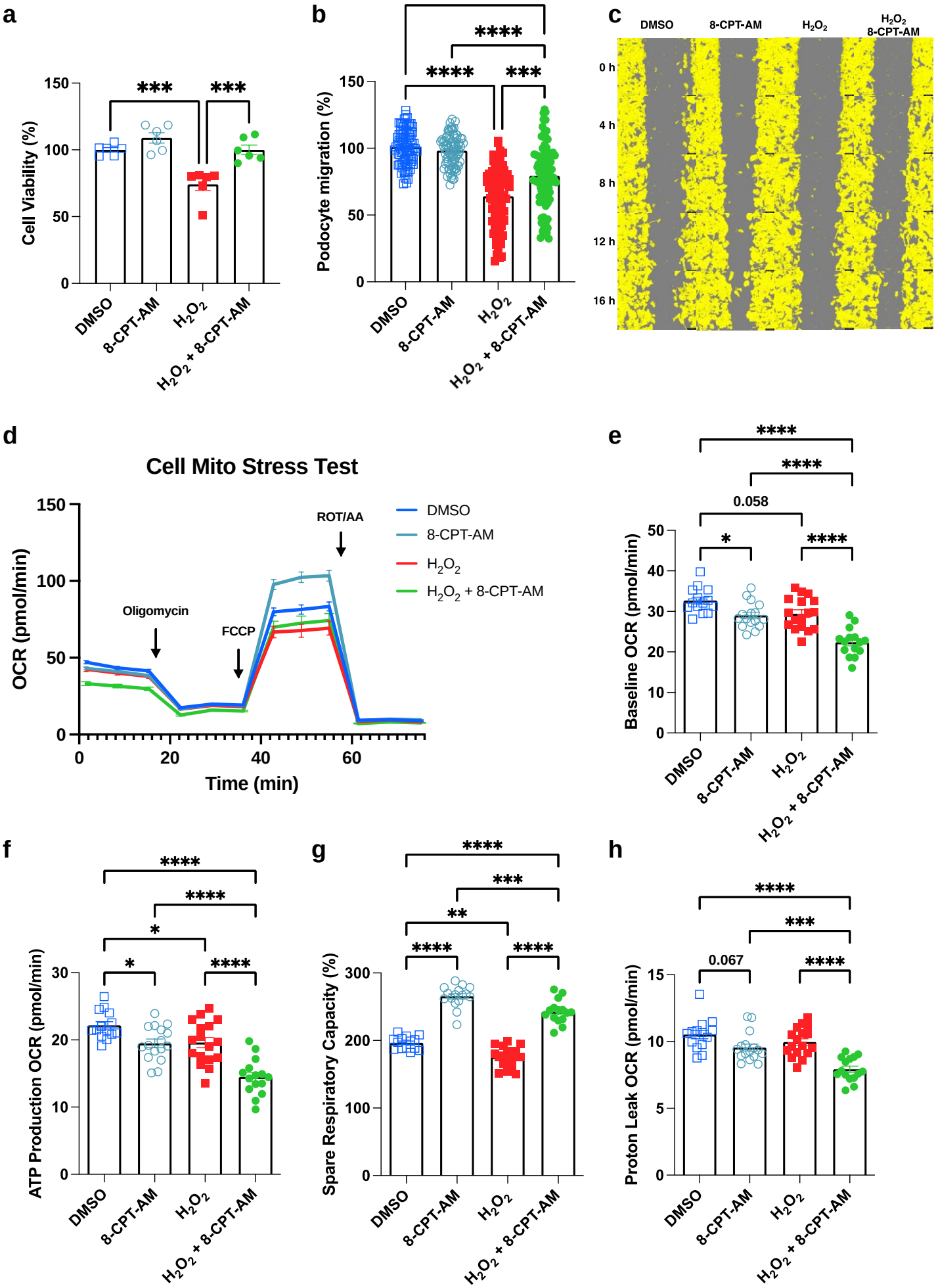
a
Cell Viability (%)
150
100
50
0
***
***
DMSO
8-CPT-AM
H2O2
H2O2 + 8-CPT-AM
b
Podocyte migration (%)
****
****
****
***
c
DMSO
8-CPT-AM
H2O2
H2O2 8-CPT-AM
0 h
4 h
8 h
12 h
16 h
d
Cell Mito Stress Test
OCR (pmol/min)
Time (min)
Oligomycin
FCCP
ROT/AA
DMSO
8-CPT-AM
H2O2
H2O2 + 8-CPT-AM
e
Baseline OCR (pmol/min)
0.058
f
ATP Production OCR (pmol/min)
g
Spare Respiratory Capacity (%)
h
Proton Leak OCR (pmol/min)
0.067

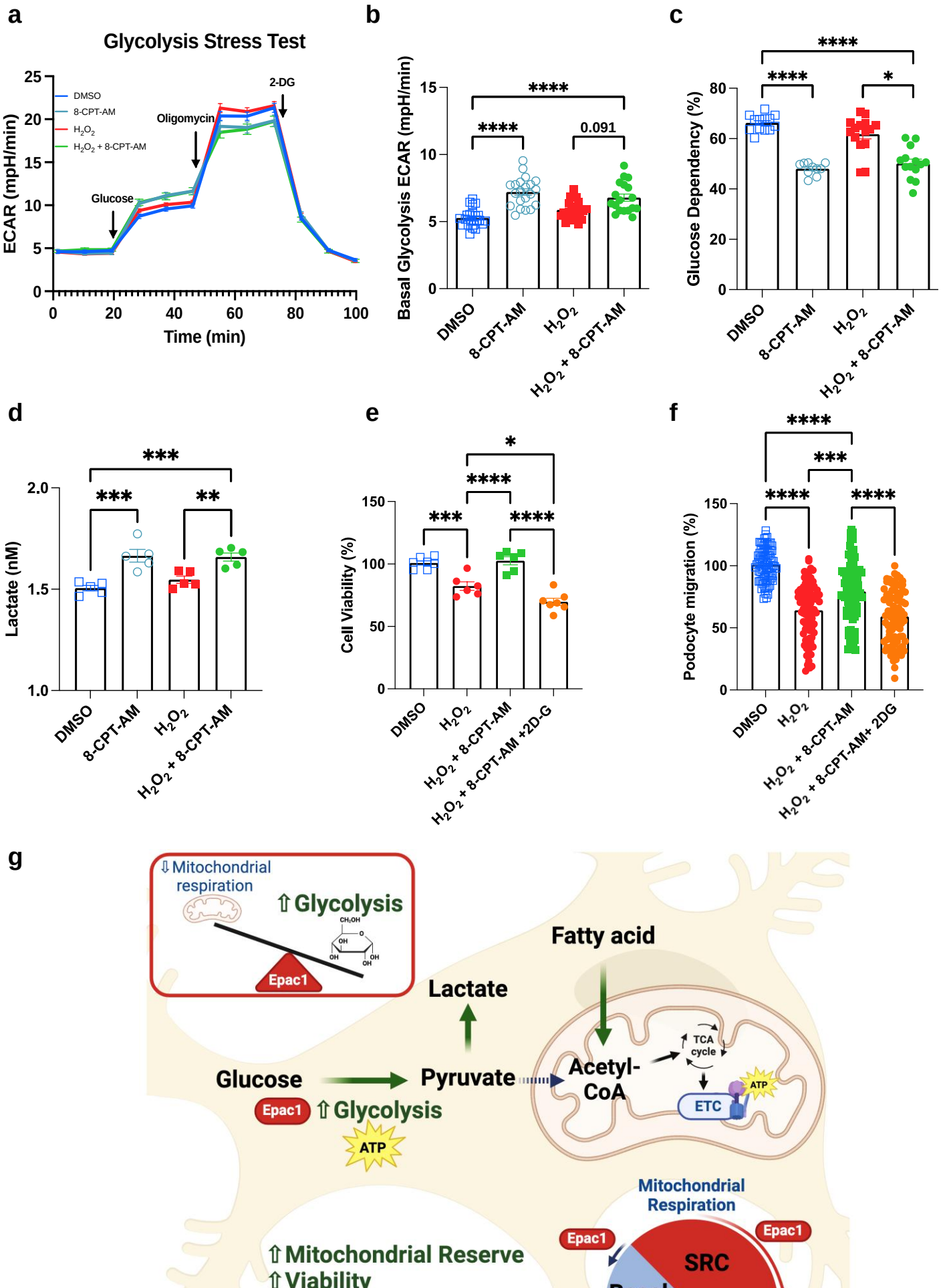
a
Glycolysis Stress Test
ECAR (mpH/min)
Time (min)
DMSO
8-CPT-AM
H2O2
H2O2 + 8-CPT-AM
Glucose
Oligomycin
2-DG
b
Basal Glycolysis ECAR (mpH/min)
****
****
0.091
DMSO
8-CPT-AM
H2O2
H2O2 + 8-CPT-AM
c
Glucose Dependency (%)
****
****
*
d
Lactate (nM)
***
***
**
e
Cell Viability (%)
*
****
***
****
H2O2 + 8-CPT-AM +2D-G
f
Podocyte migration (%)
****
***
****
****
H2O2 + 8-CPT-AM+ 2DG
g
⇩Mitochondrial respiration
⇧Glycolysis
Epac1
Fatty acid
Lactate
Glucose
Pyruvate
Acetyl-CoA
TCA cycle
ETC
ATP
⇧Glycolysis
⇧Mitochondrial Reserve
⇧Viability
⇧Motility
Mitochondrial Respiration
SRC
Basal
Max
0

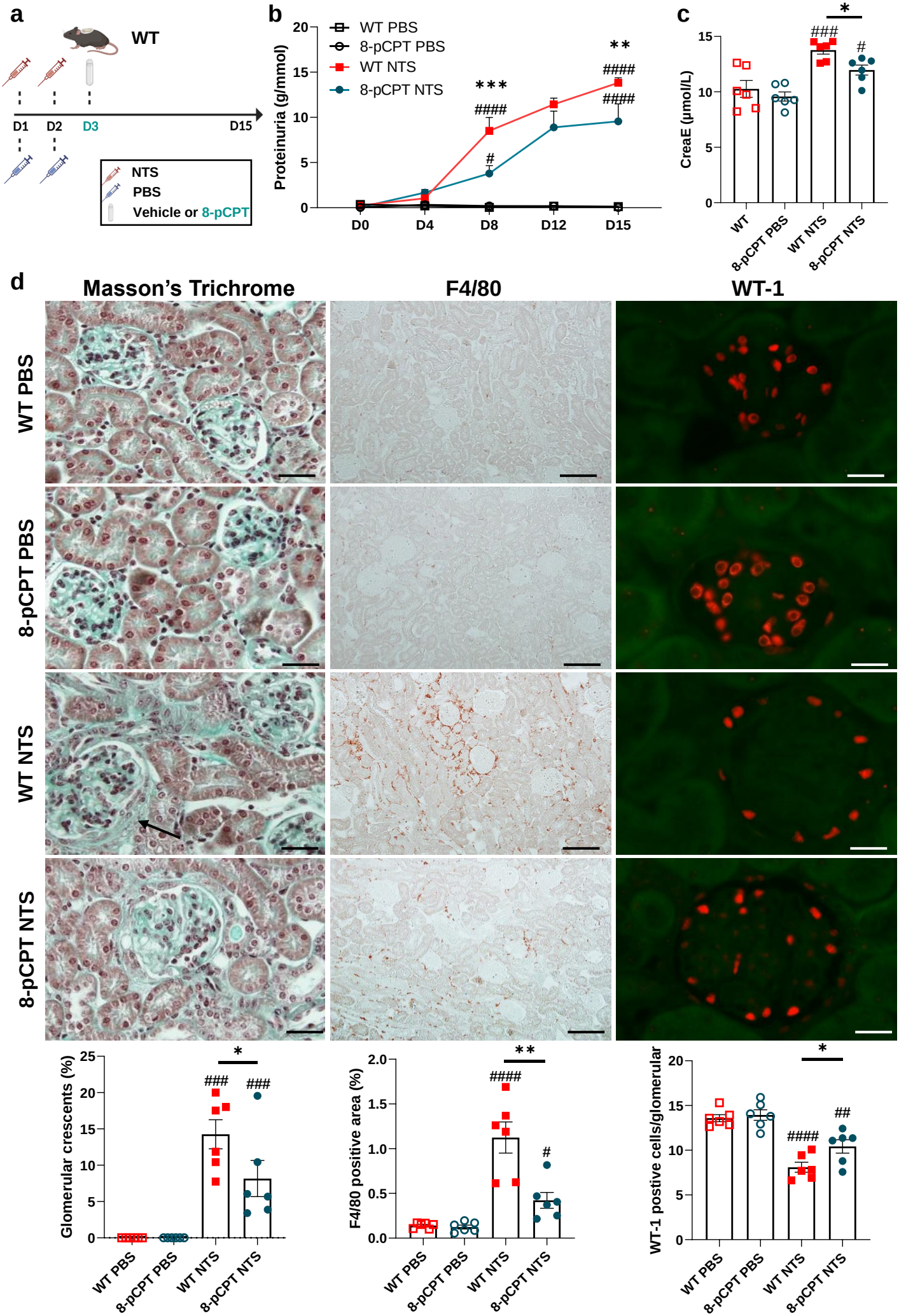
a
WT
D1
D2
D3
D15
NTS
PBS
Vehicle or 8-pCPT
b
WT PBS
8-pCPT PBS
WT NTS
8-pCPT NTS
Proteinuria (g/mmol)
D0
D4
D8
D12
D15
c
CreaE (μmol/L)
WT
8-pCPT PBS
WT NTS
8-pCPT NTS
d
Masson's Trichrome
F4/80
WT-1
WT PBS
8-pCPT PBS
WT NTS
8-pCPT NTS
Glomerular crescents (%)
F4/80 positive area (%)
WT-1 postive cells/glomerular

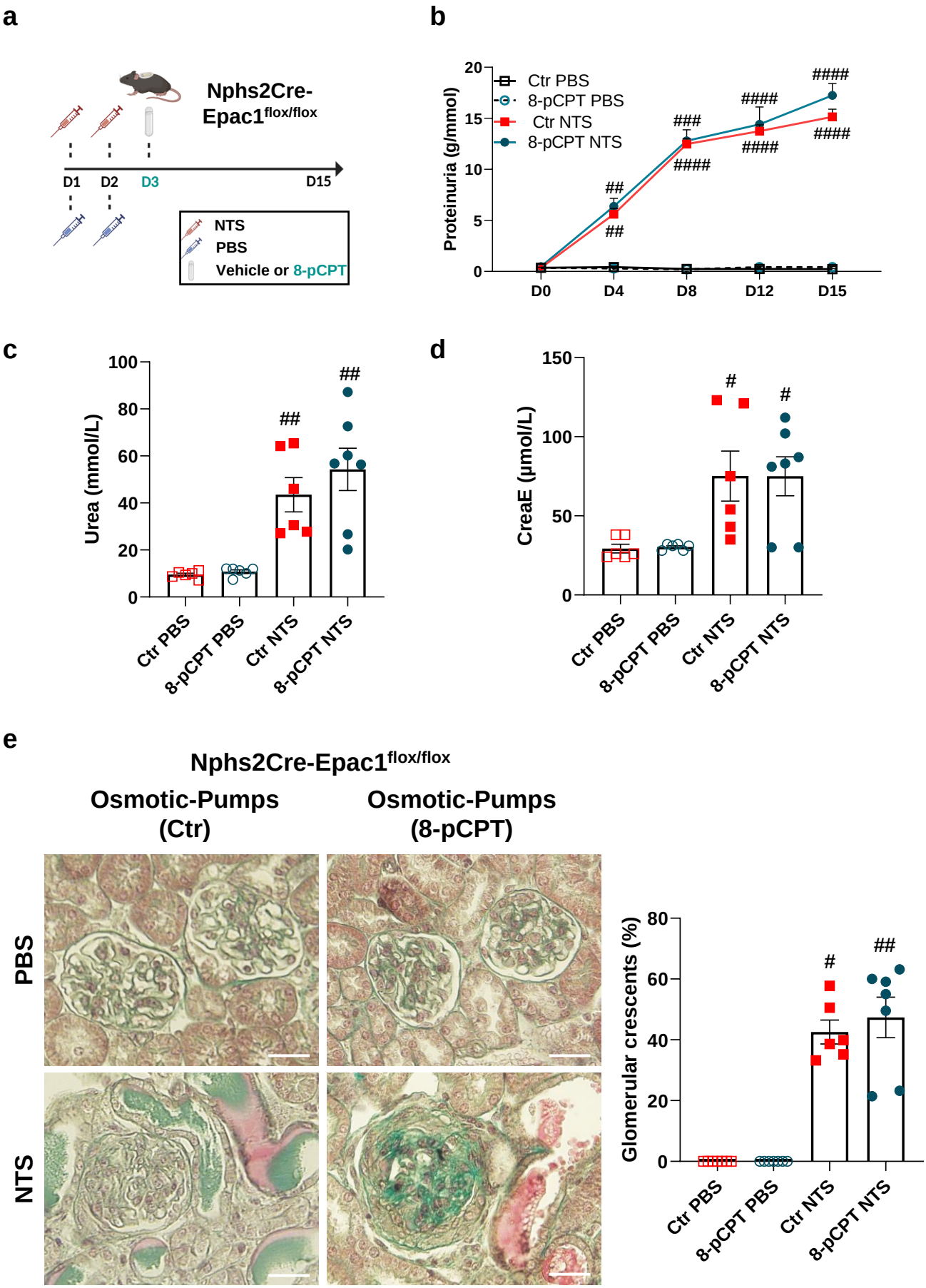
a
Nphs2Cre-Epac1flox/flox
D1
D2
D3
D15
NTS
PBS
Vehicle or 8-pCPT
b
Proteinuria (g/mmol)
Ctr PBS
8-pCPT PBS
Ctr NTS
8-pCPT NTS
D0
D4
D8
D12
D15
c
Urea (mmol/L)
Ctr PBS
8-pCPT PBS
Ctr NTS
8-pCPT NTS
d
CreaE (µmol/L)
e
Nphs2Cre-Epac1flox/flox
Osmotic-Pumps (Ctr)
Osmotic-Pumps (8-pCPT)
PBS
NTS
Glomerular crescents (%)

SUPPLEMENTARY METHODS

Animal experiments

Passive NTS-GN was performed by intravenous administration of 20 µl NTS per gram of body weight (gBW) in Epac1$^{-/-}$ mice (C57BL/6-SV129 background) and their wild-type littermates.

Conditional knockdown mice with Epac1 disruption in podocytes (*NPHS2Cre*: Epac1$^{fl/fl}$) and their littermates (Epac1$^{fl/fl}$) were also subjected to NTS or PBS injection (18,5 µl/gBW). These mice were generated by the crossbreeding of Epac1 floxed mice (B6;129S2-Rapgef3$^{tm1\ Geno/J}$) and a transgenic mouse line that expresses Cre recombinase under the podocyte-specific promoter podocin (Nphs2) on the 129S6/Sv genetic background [1].

In a separate study, C57Bl6 female mice were injected with (17 µl/gBW) of NTS. The day after the last injection, osmotic mini-pumps (Alzet model 1002) were implanted subcutaneously in mice (under anaesthesia, isoflurane 1%). Pumps were filled with either 8-(4-Chlorophenylthio)-2'-O-methyladenosine-3', 5'- cyclic monophosphate (8-pCPT) (BioLog, Germany) or vehicle (sterile PBS) and were set to deliver 8-pCPT at 3 mM (1.5 mg)/mouse/day. A similar protocol injecting NTS followed by continuous administration of 8-pCPT was applied in *NPHS2Cre*: Epac1$^{fl/fl}$ and their control littermates (Epac1$^{fl/fl}$) (n=6/7 mice per group).

All mice were euthanized 15 days after NTS/PBS administration. Urine samples were collected on days 0, 4, 8, 12, and 15. Blood samples were collected at the end of each protocol. Kidneys were fixed in AFA before paraffin embedding for immuno/histological analysis or cut in segments then snap-frozen in liquid nitrogen for RNA/protein extraction.

In the results, figures and legends, the littermates control mice for Epac1$^{-/-}$ were annotated as wild-type (WT), and for *NPHS2Cre*: Epac1$^{fl/fl}$ as control (Ctr).

The number of mice per strain and/or samples for each experimental setting is listed in Figure Legends.

Assessment of renal function

Proteinuria was measured with a Konelab automater (Thermo Fisher Scientific) and normalized to urine creatinine. Blood urea and creatinine levels were measured with an enzymatic method (Konelab automater). The measurements were carried out within the "Small Animal Renal Explorations" platform located at the Cordelliers Research Center, Paris. This platform specializes in the biochemical analysis of rodents.

Histology

AFA-fixed, paraffin-embedded, kidney (4 µm) sections were stained with Masson Trichrome for histologic evaluation. Crescent formation was evaluated double-blinded on coded slides as percentage of injured glomeruli with crescents per total glomeruli examined.

Transmission electron microscopy

Mouse kidneys tissues were cut into small slices and fixed in 2.5% glutaraldehyde in 0.1 mol/L cacodylate buffer then post fixed in 1% OsO4. Kidney slices were then embedded in epoxy resin. Semi-thin sections (0.5 mm) were counterstained with toluidine blue and the ultrathin sections (80 nm) with uranyless and lead citrate. At least 3 glomeruli and 10 capillary loops per glomerulus were viewed and analyzed with JEOL1010 electron microscope.

Immunostaining

Staining was performed on 4 µm deparaffinised tissues and heat-induced epitope retrieval with Citrate (pH=6.1), excepted for the Wilms's tumor 1 gene (WT1) and CD44 staining made with Tris-EDTA (pH=9). For immunohistochemistry, sections were incubated with F4/80 (Abserotec)), KIM-1 (R&D Systems), Epac1 (Merck) and collagen I (Abcam). For immunofluorescence slides were incubated with anti-goat (Invitrogen), anti-mIgG (Invitrogen), or incubated with primary antibody WT1 (Abcam), Epac1 (Merck),), α-SMA (Abcam) and nestin (Abcam). Images were obtained with an Olympus IX83 microscope and quantified with ImageJ (free access NIH software).

Western Blot analysis

Protein extracts from total kidney tissues or podocytes were separated by SDS-polyacrylamide gel electrophoresis and transferred to polyvinylidene difluoride membranes (Millipore). The membranes were incubated with the primary antibody for Epac1(Abcam), GAPDH (Sigma), followed by incubation with peroxidase-conjugated secondary antibodies (Bio-Rad). Membranes were revealed with luminol-based chemiluminescent substrate (ECL Clarity, Bio-Rad). Signals were quantified by densitometry using the Image Lab software (Bio-Rad).

Total RNA isolation and real-time quantitative RT-PCR

Total RNA was extracted from kidneys using TRIzol reagent (Euromedex). One microgram of total RNA was reverse transcribed in cDNA. Quantitative RT-qPCR was performed with an SYBR Green kit (Roche, Boulogne-Billancourt, France) on a CFX96 RT-PCR Detection System (Bio-Rad, Marnes-la-Coquette, France). Analysis of relative gene expression was performed by using the ($2^{-\Delta\Delta CT}$) method and normalised by housekeeping genes (RPL32

and HPRT). Results are expressed in graphs as arbitrary units, which represent the ratio of relative gene expression normalized to control mice. Primer sequences are listed below.

Col1	GCAGGTTCACCTACTCTGTCCT	CTTGCCCCATTCATTTGTCT
HPRT	GGAGCGGTAGCACCTCCT	CTGGTTCATCATCGCTAATCAC
MCP-1	AGCTTCATCGAACCATTAGCAGAA	CCTTCTAGGTCCTGTACGTGGA
NGAL	CCATCTATGAGCTACAAGAGAACAA	TCTGATCCAGTAGCGACAGC
RPL32	GCTGCCATCTGTTTTACGG	TGACTGGTGCCTGATGAACT
V-CAM	TGGTGAAATGGAATCTGAACC	CCCAGATGGTGGTTTCCTT

RNA sequencing, data processing and differential expression analysis

After extraction from glomeruli, total RNA was qualified with AGILENT tapeStation 2200. RNA library preparation was performed following manufacturer's recommendations (QuantSeq 3' mRNA-Seq Library Prep Kit FWD for Illumina from LEXOGEN). Final sample pooled library preparation was sequenced on ILLUMINA Novaseq 6000, corresponding to 1 x 36 Millions of 100 bases read per sample after demultiplexing. Quality of raw data was evaluated with FastQC[2]. Poor quality sequences and adapters were trimmed or removed with fastp tool[3], with default parameters, to retain only good quality paired reads. Illumina DRAGEN bio-IT Plateform (v3.8.4) was used for mapping on mm10 reference genome and quantification with gencode vM25 annotation gtf file. Library orientation and composition and coverage along transcripts were checked with Picard tools. Following analyses were conducted with R software. Data were normalized with DESeq2 (v1.26.0) bioconductor packages[4], prior to differential analysis with glm framework likelihood ratio test from DESeq2 workflow. Multiple hypothesis adjusted p-values were calculated with the Benjamini-Hochberg procedure to control FDR. Finally, enrichment analysis was conducted with topGO (v2.46.0.) bioconductor packages using the weight01 algorithm which allows accounting for the hierarchical structure of GO (Gene Ontology) and Kolmogorov-Smirnov

(KS) statistical test using FDR as rank[5]. GO annotations were obtained from the R package org.Mm.eg.db (Bioconductor 3.14). GO databases, biological process, molecular function and cellular compartment were used for the analysis. All the genomics data are available through GEO repository with accession number GSE237097 (as the data are private until publication, please find the token for reviewers: ezurcsgujbwjter).

Measurements of oxygen consumption and extracellular acidification rate

An Agilent Seahorse XF Pro Analyzers was used to measure the rate change of dissolved O_2 and pH in medium immediately surrounding adherent cells cultured in a Seahorse XFe96 Analyzer 96-well plate (Seahorse Agilent, Santa Clara, CA, USA). Differentiated podocytes were trypsined and seeded in XFe96-well microplates at 1.0×10^4 cells. Cells were pre-treated with 8-CPT-AM (10 μM) or vehicle (DMSO)- then stimulated or not for 4 hours with H_2O_2 (150 μM) To assess mitochondrial function, Seahorse Cell Mito Stress Test was performed. Oxygen consumption rate (OCR) was evaluated at basal state and then following the sequential injection of oligomycin (1 μM), carbonyl cyanide-4 (trifluoromethoxy) phenylhydrazone (FCCP, 4 μM), and antimycin A (1 μM) plus rotenone (1 μM). This test allows the measurement of basal respiration, ATP production linked to respiration, maximal/spare respiration and proton leak. To assess the capacity of the glycolytic pathway, Seahorse Glycolysis Stress Test was performed. After glucose starvation, extracellular acidification rate (ECAR) was evaluated without glucose in the assay medium, then glucose (10 mM), oligomycin (1 μM), and 2-Deoxy-d-glucose (2-DG, 50 mM) was injected. To assess the oxidation rate of glucose and fatty acid, we performed the Seahorse Mito Fuel Flex Test in the presence or absence of fuel pathway inhibitors. Three inhibitors are used after baseline OCR measurement. For glucose dependency, UK-5099 (2 μM) is injected followed by co-injection of BPTES (3 μM) and Etomoxir (4 μM). For fatty acid dependency, Etomoxir

(4 µM) is injected followed by co-injection of UK-5099 (2 µM) and BPTES (3 µM). The results were automatically calculated, recorded, and plotted by Seahorse Wave Pro Software version 10.1.0.1.

Podocyte cell culture and viability test

AB8/13, a human conditionally immortalized podocyte cell line, was maintained as previously described[6] at 33°C and differentiated at 37°C. Cells were then seeded in 96-well plate, and were pre-treated with 8-CPT-AM or vehicle (DMSO)- then stimulated or not for 3 hours with H_2O_2 (200µM). To measure cell viability the supernatant was removed and replaced by CellTiter-Blue agent (Promega). The percentage of viable cell was normalized to controls.

Scratch assay

Confluent cells on six-well plates were scratched with a 200 µl sterile pipette. Then differentiated podocytes were treated with H_2O_2 (200 µM) treatment for 24 hours, 8-CPT-AM (10 µM) is added 30 min before and during the H_2O_2 treatment. Images were obtained with the Incucyte S3 (Sartorius). By comparing the images from 0 and 24 h the percentage of closure was calculated from confluence detection with Incucyte algorithm.

Lactate Assay

The lactate concentration was determined by enzymatic assay according to manufacturer's instructions (lactate Assay Kit, Abcam) on deproteinized cell culture supernatants.

SUPPLEMENTARY FIGURES

Figure S1

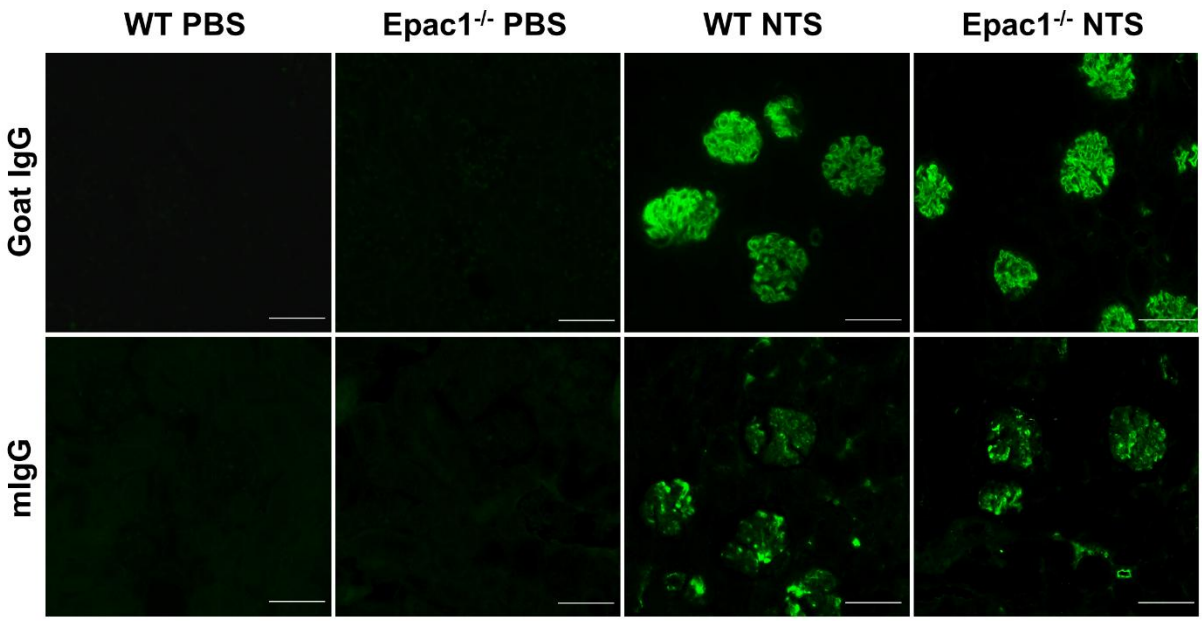

Supplementary Figure S1. **Renal goat and mouse IgG deposits in WT and Epac1$^{-/-}$ mice**. Representative immunostaining showing goat IgG and mouse IgG (mIgG) deposits on kidney sections of WT PBS, Epac1$^{-/-}$ PBS, WT PBS and Epac1$^{-/-}$ NTS. (Scale bar=50 µM).

Figure S2

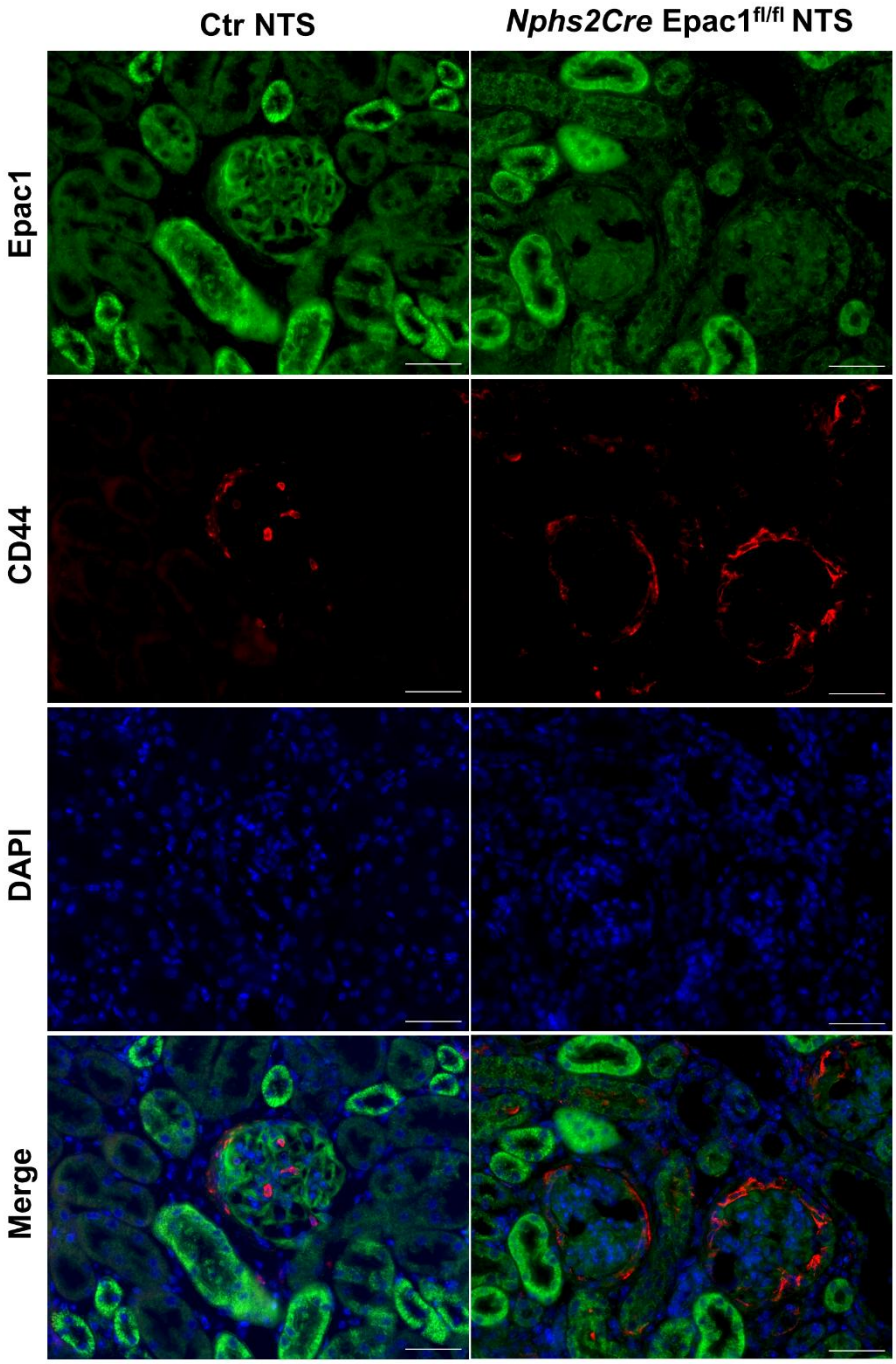

Supplementary Figure S2. **Co-immunostaining of Epac1 and CD44 in the renal cortex of Ctr and *Nphs2Cre*-Epac1$^{fl/fl}$ mice after NTS**. Representative image of CD44 and EPAC1 co-immunostaining in kidney of Ctr NTS and *Nphs2Cre*-Epac1$^{fl/fl}$ NTS mice. Eapc1 (green), CD44 (red), DAPI (bleu). Scale bar=50 µM.

Figure S3

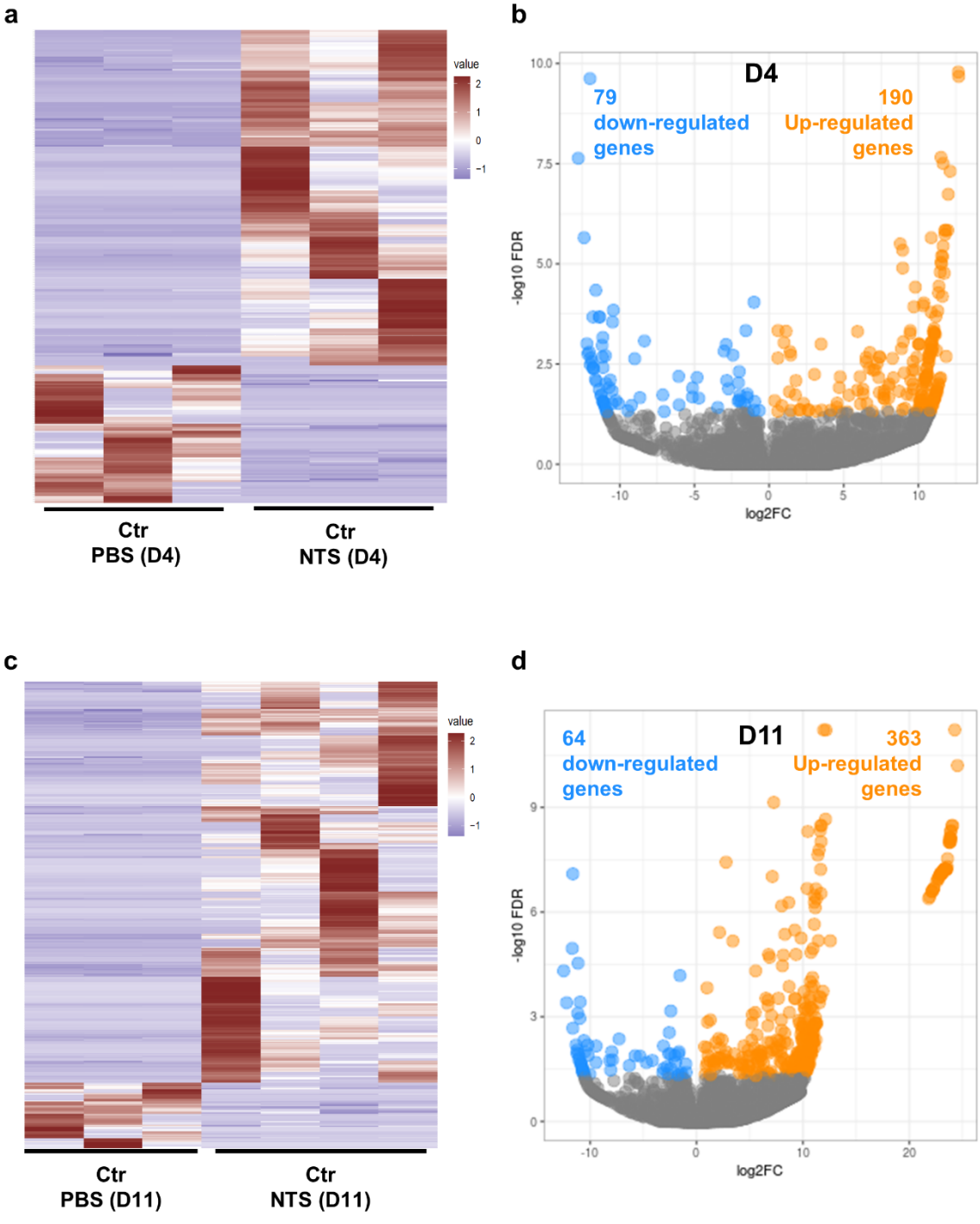

Supplementary Figure S3. Transcriptomic signature in glomeruli underlying NTS-induced GN. (**a**) Heatmap showing hierarchical clustering of differentially expressed genes (FDR < 0.05) between Ctr PBS and Ctr NTS D4 groups (n = 3-4 biological replicates per

group). (**b**) Volcano plot of differentially expressed genes between Ctr PBS and Ctr NTS D4 groups sorted according to fold change and significance (FDR < 0.05). (**c**) Heatmap showing hierarchical clustering of differentially expressed genes for Ctr PBS and Ctr NTS D11 groups (n = 3-4 biological replicates per group). (**d**) Volcano plot of differentially expressed genes between Ctr PBS and Ctr NTS D11 groups sorted according to fold change and significance (FDR < 0.05).

Figure S4

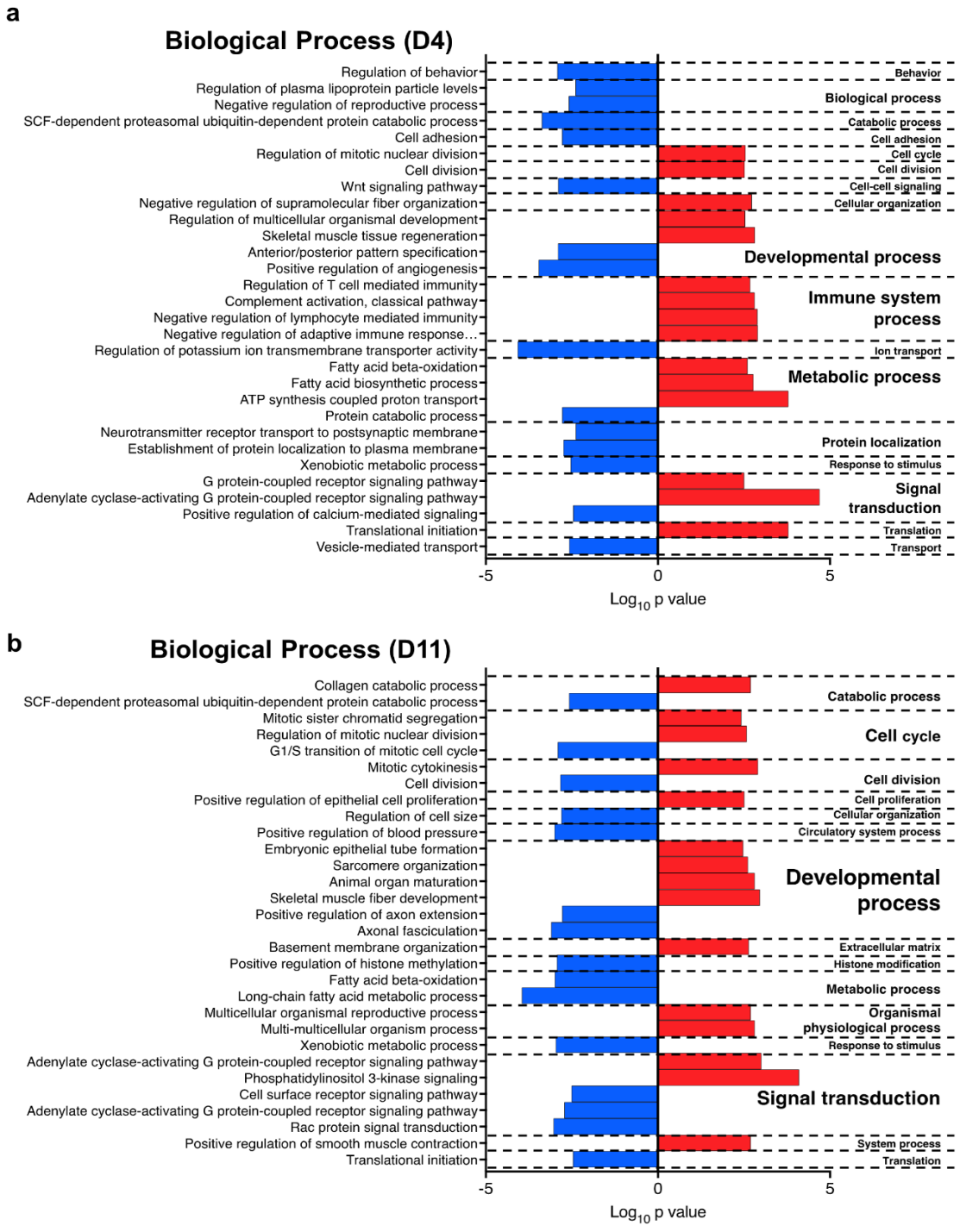

Supplementary Figure S4. Transcriptomic signature of biological process in glomeruli underlying NTS-induced GN. (**a**) Enrichment analysis of biological process gene ontology terms for differentially regulated genes in Ctr PBS vs Ctr NTS D11 D4 and (**b**) D11. Up-regulated and down-regulated genes in Ctr PBS vs Ctr NTS are represented in red and blue, respectively.

Figure S5

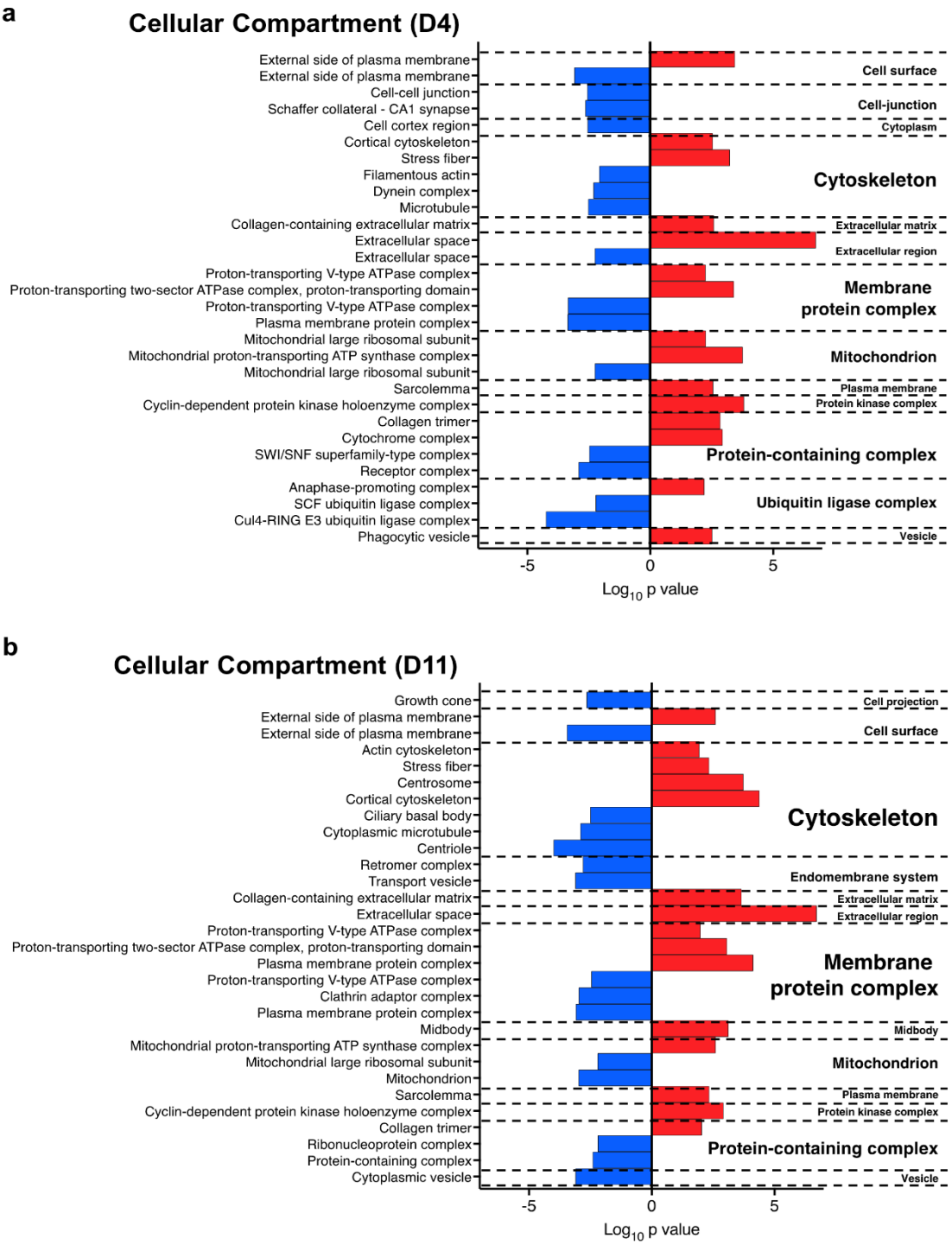

Supplementary Figure S5. Transcriptomic signature of cellular compartment in glomeruli underlying NTS-induced GN. (**a**) Enrichment analysis of cellular compartment gene ontology terms for differentially regulated genes on D4 and (**b**) D11. Up-regulated and down-regulated genes in Ctr PBS vs Ctr NTS are represented in red and blue, respectively.

Figure S6

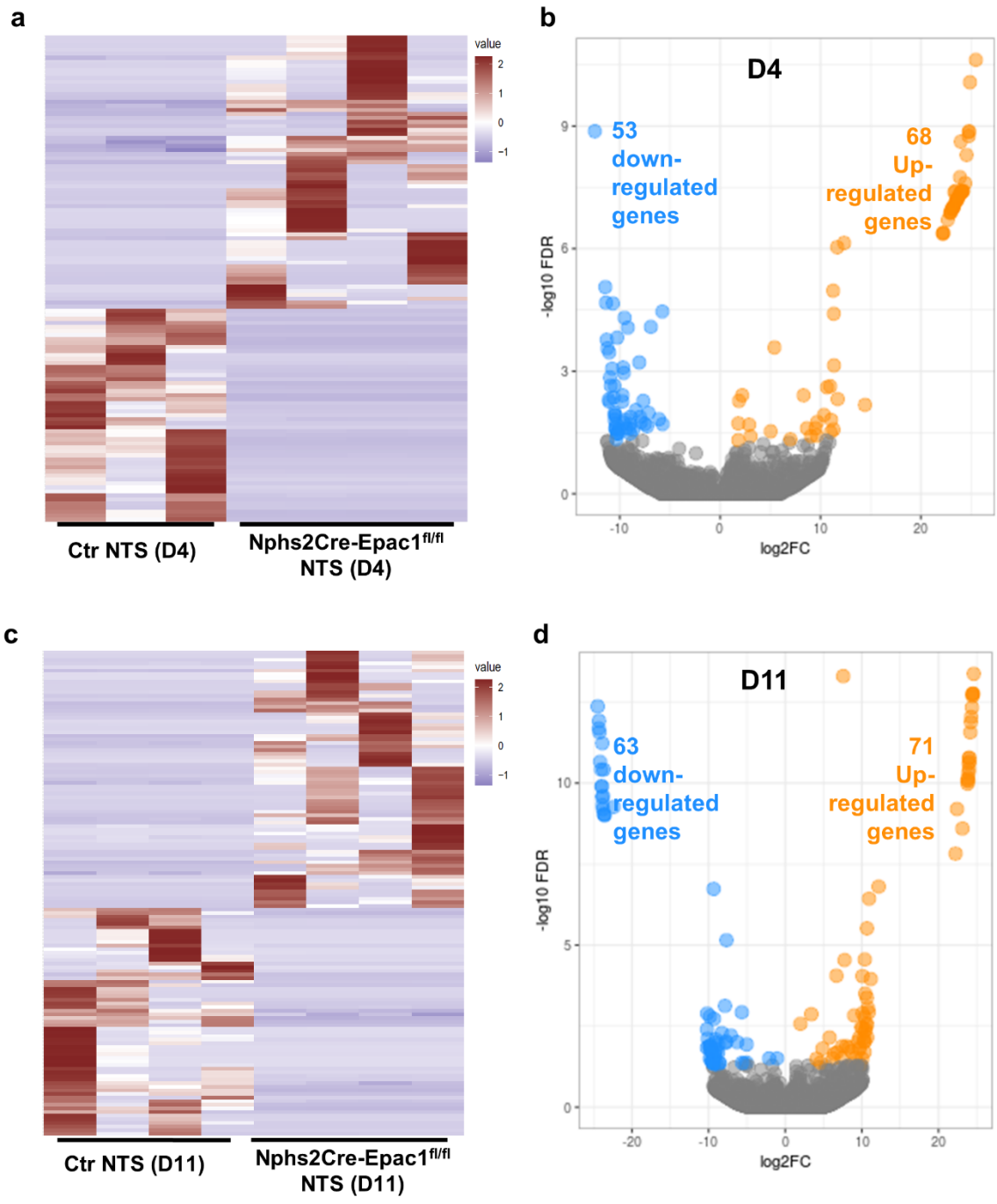

Supplementary Figure S6. Heatmap and Volcano plot of differentially expressed genes in glomeruli of Ctr NTS and *Nphs2Cre*-Epac1$^{fl/fl}$ mice at D4 and D11. (**a**) Heatmap showing hierarchical clustering of differentially expressed genes at D4 (FDR < 0.05) between Ctr NTS and *Nphs2Cre*-Epac1$^{fl/fl}$ NTS groups (n = 3-4 biological replicates per group). (**b**)

Volcano plot of differentially expressed genes (D4) between Ctr NTS and *Nphs2Cre*-Epac1$^{fl/fl}$ groups sorted according to fold change and significance (FDR < 0.05). (**c**) Heatmap showing hierarchical clustering of differentially expressed genes at D11 for Ctr NTS and *Nphs2Cre*-Epac1$^{fl/fl}$ groups (n = 3-4 biological replicates per group). (**d**) Volcano plot of differentially expressed genes D11 between Ctr NTS and *Nphs2Cre*-Epac1$^{fl/fl}$ groups sorted according to fold change and significance (FDR < 0.05).

Figure S7

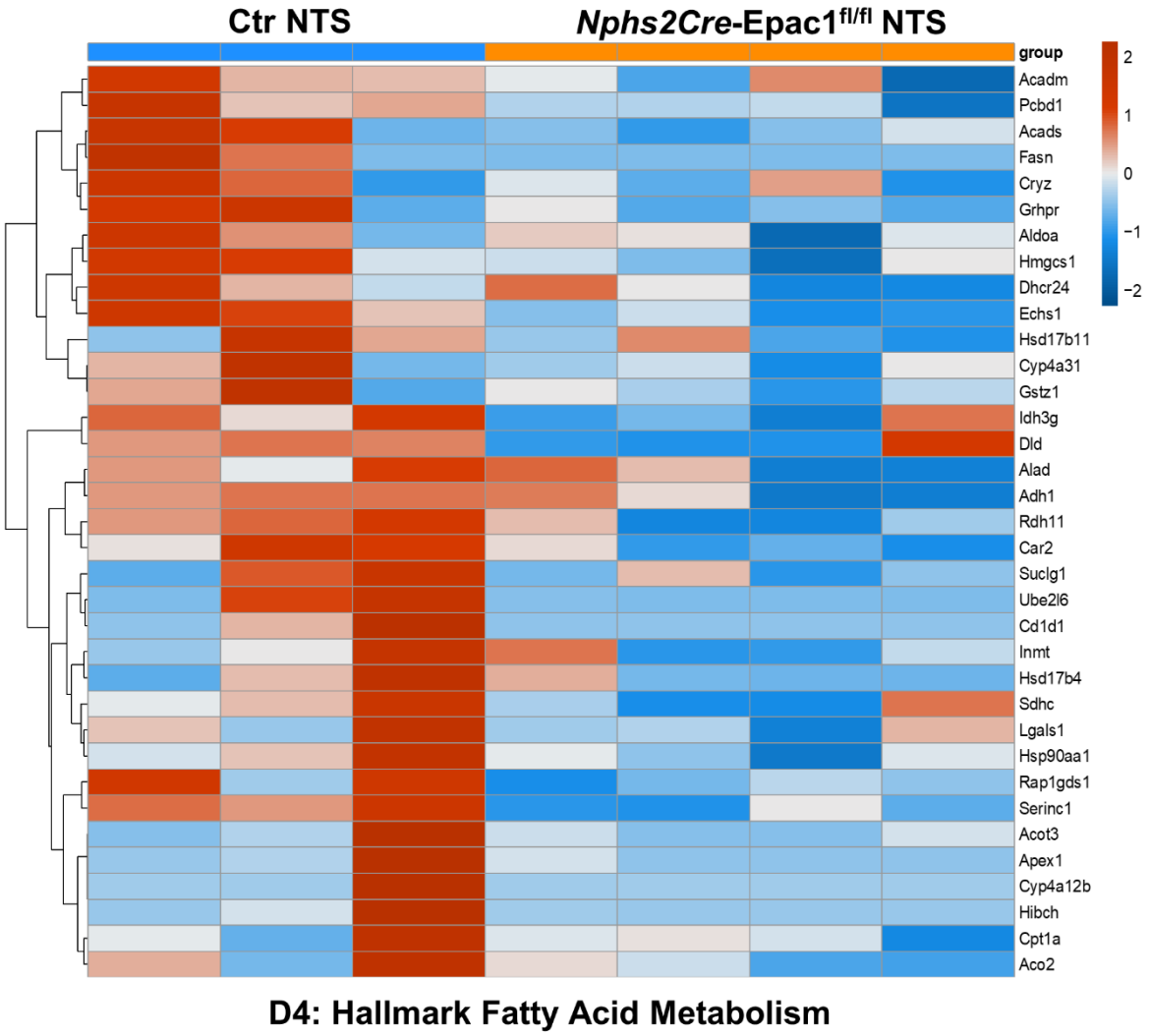

Supplementary Figure S7. Epac1 inhibition dysregulates fatty acid pathway at the onset of GN. Heatmap showing differentially regulated genes on D4 between Ctr NTS and *Nphs2Cre*-Epac1$^{fl/fl}$ NTS related to the fatty acid metabolism (FDR < 0.05).

Figure S8

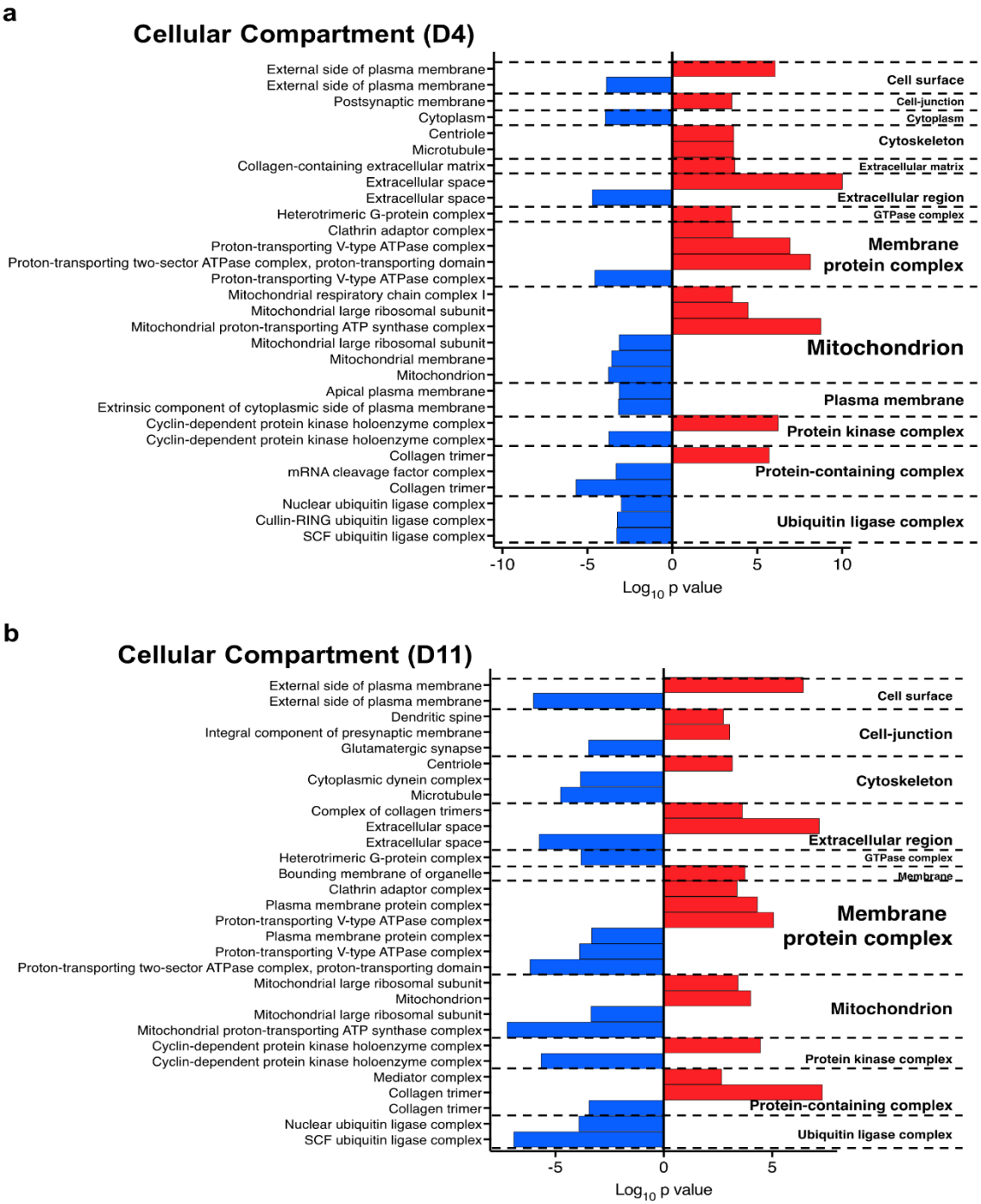

Supplementary Figure S8. Epac1 inhibition targets mitochondria at the onset of GN. (**a**) Enrichment analysis of cellular compartment gene ontology terms for differentially regulated genes on D4 and (**b**) D11. Up-regulated and down-regulated genes in *Nphs2Cre*-Epac1$^{fl/fl}$ NTS vs. Ctr NTS are represented in red and blue, respectively.

Figure S9

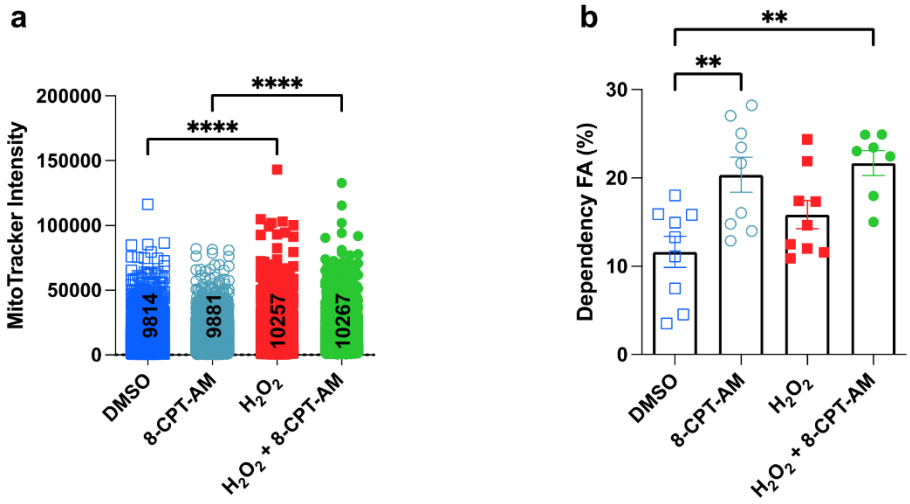

Supplementary Figure S9. Epac1 drives a metabolic switch without affecting the number of mitochondria. (**a**) Graph of MitoTracker intensity assessed by flow cytometry representing the amounts of mitochondria, n=2 experiments, around 10 000 cells/experiment/group, the mean of each group is displayed on the graph (like seahorse experiments, 4 h treatment, H_2O_2: 150 µM; 8-CPT-AM:10 µM). (**b**) Fatty acid dependency, with the Seahorse Mito Fuel Flex test, is the percentage of OCR related to fatty acid oxidation in the mitochondria (Etomoxir inhibits carnitine palmitoyl-transferase 1A, 4 µM). Total OCR inhibition was performed in presence of glucose and glutamate oxidation inhibitors (UK-5099, 2 µM for mitochondrial pyruvate carrier inhibition and BPTES, 3 µM for allosteric inhibition of glutaminase converting glutamine to glutamate), (n=7-8 biological replicates). If normality is respected one-way ANOVA followed by Tukey test is performed, if not, Kruskall Wallis test followed by Dunn's test is done. ***P*<0.01, *****P*<0.0001.

SUPPLEMENTARY REFERENCES

1. Moeller, M. J., Sanden, S. K., Soofi, A., Wiggins, R. C. & Holzman, L. B. Podocyte-specific expression of cre recombinase in transgenic mice. *Genesis*. 2003; 35: 39–42.
2. Andrew, S. FastQC: a quality control tool for high throughput sequence data. 2010.
3. Chen, S., Zhou, Y., Chen, Y. & Gu, J. fastp: an ultra-fast all-in-one FASTQ preprocessor. *Bioinformatics*. 2018; 34: i884–i890.
4. Love, M. I., Huber, W. & Anders, S. Moderated estimation of fold change and dispersion for RNA-seq data with DESeq2. *Genome Biol.* 2014; 15: 550.
5. Alexa, A. & Rahnenfuhrer, J. topGO: Enrichment Analysis for Gene Ontology. R package version 2.46.0, 2021.
6. Saleem, M. A. *et al.* A Conditionally Immortalized Human Podocyte Cell Line Demonstrating Nephrin and Podocin Expression. *J. Am. Soc. Nephrol.* 2002; 13: 630–638.